Journal of Petroleum Science and Engineering 198 (2021) 108225

Contents lists available at ScienceDirect

Journal of Petroleum Science and Engineering

journal homepage: http://www.elsevier.com/locate/petrol

# Evaluation of shale gas reservoirs in complex structural enclosures: A case study from Patala Formation in the Kohat-Potwar Plateau, Pakistan

Qamar Yasin [a,b], Syrine Baklouti [c], Perveiz Khalid [d,*], Syed Haroon Ali [e], Cyril D. Boateng [a], Qizhen Du [a,b,**]

[a] The Key Laboratory of Deep Oil and Gas, China University of Petroleum (East China), PR China
[b] The Laboratory for Marine Mineral Resources, Qingdao National Laboratory for Marine Science and Technology, Qingdao, 266071, China
[c] University of Sfax, National School of Engineers (ENIS), Laboratory of Environmental Engineering and Eco-Technology, Route de Soukra Km 3, 5, Po. Box 1173, 3038, Sfax, Tunisia
[d] Institute of Geology, University of the Punjab, Lahore, Pakistan
[e] Department of Earth Sciences, University of Sargodha, Sargodha, 40100, Pakistan

ARTICLE INFO

*Keywords:*
Kohat-potwar plateau
Patala formation
Shale gas
Rock-eval pyrolysis
Petrophysics

ABSTRACT

Breakthroughs in shale gas exploration and production technology in China point to a possible solution to Pakistan's current energy crises. In this study, we evaluate the shale gas prospects in the Kohat-Potwar Plateau of Pakistan by establishing an integrated approach involving the analysis of fundamental elastic and petrophysical properties, Rock-Eval pyrolysis, and the sealing mechanism of shale. Detailed geochemical and petrophysical evaluation of the Patala Formation in the Kohat-Potwar Plateau indicates the good potential for shale gas with the following characteristics similar to the Longmaxi shale of Sichuan Basin China, i.e., (i) complex structural types sandwiched by tight limestone strata with low porosity (less than 3%), ultra-low permeability, high density, and large thickness which provides strong sealing capacity for gas preservation and enrichment; (ii) multiphase tectonic evolution of Patala Formation allowed various slippage processes to develop fractures and enhance the porosity and permeability; (iii) high organic matter content and thermal maturation stage (TOC > 2%, 416–445 °C); (iv) high brittle minerals content (e.g., calcite and dolomite > 40%); and (v) large formation thickness (>30 m) at shallow burial depth < 2500 m. This study emphasizes the critical role of the sealing mechanism in shale gas reservoirs. Furthermore, the results suggest that the evaluation and development of shale gas potential using petrophysical and geochemical analysis may be inadequate. Further scrutiny of the roof and floor of reservoirs' efficient sealing capacities is essential to understand the extent of shale gas preservation and enrichment. The study results provide valuable insights for identifying the sweet spots and preservation condition of shale gas in the Kohat-Potwar Plateau of Pakistan.

## 1. Introduction

Characterizing organic-rich shales for petroleum exploration is still challenging due to inherently low porosity and ultra-low permeability, presence of platy clay minerals and compliant organic matter, stiff mineral grains, differentiation of brittle and ductile zones, and structural instability and preservation conditions (Yasin et al., 2018). These fundamental properties are necessary for the selection and development of a new shale gas play. Besides, organic matter content, kerogen porosity, and minerals play a significant role in the velocity, density, and resistivity of shales. Therefore, a typical suite of wireline logs could be useful for the determination of such petrophysical properties (Sohail et al., 2020).

Shale reservoirs usually exhibits ultra-low permeability, which requires the utilization of sequenced multi-stage hydraulic fracturing technology to achieve economic gas production rates (Li et al., 2018). The multi-stage hydraulic fracturing treatment generates a complex fracture network that connects with pre-existing fractures to produce gas from the rock matrix and ultimately enhances production. However, before this, it is necessary to understand the shale's brittle and ductile

* Corresponding author.
** Corresponding author. The Key Laboratory of Deep Oil and Gas, China University of Petroleum (East China), PR China.
*E-mail addresses:* qamarquaidian@gmail.com (Q. Yasin), syrine.baklouti.mtibaa@gmail.com (S. Baklouti), perveiz.geo@pu.edu.pk, perveiz.geo@pu.edu.pk (P. Khalid), geologyuos@gmail.com (S.H. Ali), cyrilboat@yahoo.com (C.D. Boateng), multicomponent@163.com, multicomponent@163.com (Q. Du).

https://doi.org/10.1016/j.petrol.2020.108225
Received 17 August 2020; Received in revised form 17 November 2020; Accepted 2 December 2020
Available online 5 December 2020

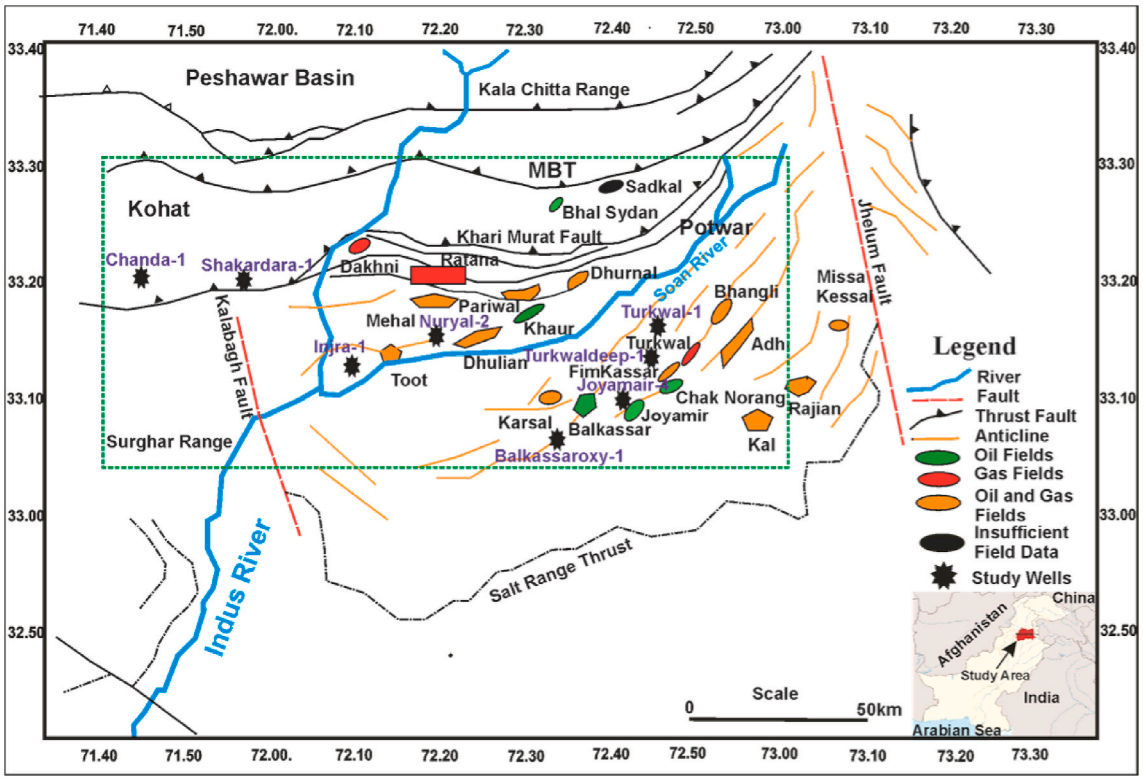


**Fig. 1.** Structural maps of Kohat-Potwar Plateau, indicating the location of study area (highlighted with doted green box) and oil and gas fields (modified after Shah, 2009; Khalid et al., 2014). (For interpretation of the references to color in this figure legend, the reader is referred to the Web version of this article.)

behavior (Yasin et al., 2017). In this context, the term 'brittleness' is often used to describe an attribute that characterizes a rock's tendency to hydraulically fracture (Shia et al., 2016; Kim et al., 2017).

There have been many studies on the petrophysical and geochemical characterization of shale gas reservoirs (Alexeyev et al., 2017; Iqbal et al., 2018; Sharma and Sircar, 2018; Sohail et al., 2020). However, the sealing mechanism of the roof (top) and floor (bottom) together, as an essential parameter for shale gas preservation and enrichment in complex structural enclosures, has not received enough attention. In this paper, we refer to the roof and floor as impermeable overlying and underlying stratum for sealing hydrocarbons contained within the shale gas reservoir (Tang et al., 2020). The mudstone, shale, and tight limestone could be the roof and floor layers (Guo and Zeng, 2015; Tang et al., 2020). An unstable stratum of the roof and floor can easily disperse the hydrocarbons from shale and damage the shale reservoir preservation conditions (Zhang et al., 2019a,b). Thus, it is important to study the shale sealing mechanism and its controlling factors to evaluate the prospective zone where shale gas reservoirs are preserved (Tang et al., 2019).

In the past, researchers have studied the preservation conditions of shale gas and sealing of caprocks (roof). Downey (1984) introduced the sealing capacities of caprocks and reported that effective caprocks are naturally plastic, having an adequate thickness, high capillary pressure, and excellent lateral continuity. Subsequently, many other authors investigated the sealing mechanism of caprocks in the roof and divided it into physical sealing, overpressure sealing, hydrocarbon concentration sealing, and hydraulic sealing (Watts, 1987; Huang and Hao, 1996; Yu et al., 2011; Fu et al., 2018). Later, Almon et al. (2002) investigated how shales with well-laminated, slightly silty, calcareous, and claystone have significantly greater critical seal pressures and sealing capacity. Recently, some authors have initiated the evaluation of the sealing mechanism of the roof and floor together as a whole. They have reported for Longmaxi shale gas reservoir as example, that the roof and floor with high density and high breakthrough pressure are preconditions for shale gas enrichment (Song et al., 2017; Wei et al., 2017; Guo et al., 2017; Jin et al., 2018; Zhang et al., 2019a,b). The outcome of their studies indicates that the permeability of the roof and floor set is vital for shale gas conservation. They also reported that good sealing capacities of roof and floor do not only maintain formation pressure to promote gas absorption but also reduce the loss of free gas.

Elastic properties such as Poisson's ratio, Young's modulus, shear and bulk modulus are key parameters for studying sealing capacity. They are affected by clay minerals, porosity, organic matter, and fluid saturation. Therefore, an integrated study which includes the petrophysical, elastic, and geochemical analysis as well as the sealing mechanism of roof and floor will help to optimize both reservoir characterization and shale preservation conditions evaluation (Zagorski et al., 2012).

Ayaz et al. (2012) and Ali et al. (2017) have shown that marine deposits of the late Paleocene Patala Formation are potentially important unconventional shale oil/gas reservoirs in the Kohat-Potwar Plateau of Pakistan. It is one of the complex tilted region in northern Pakistan with complicated structural attributes, i.e., moderate-steeper dip due to multiple uplifting events, thrust-wrench tectonic, normal faulting and folding (Pogue et al., 1999; Paracha, 2004; Khan et al., 2018; Ghazi et al., 2020). The dark black carbonaceous and coal beds in Patala Formation acted as important source rocks for Eocene reservoirs, especially in Potwar Plateau (Wandrey et al., 2004). This carbonaceous (organic-rich) black shale is highly fossiliferous and present in the Salt Range, Kala-Chitta Range, Kohat and Hazara exposure (Wandrey et al., 2004).

Correspondingly, the upper Ordovician Wufeng Formation and lower Silurian Longmaxi (WF-LM) Formation in the Sichuan Basin China has emerged as a viable commercial shale gas play with a production capacity of more than $7.0 \times 10^9$ $m^3/t$ and 3.14 $m^3/t$ in Fuling and Jiaoshiba shale gas fields, respectively (Yasin et al., 2018). Recently, Wu et al. (2016) reported that the Longmaxi shale has enormous unconventional resources compared to conventional plays in China. This

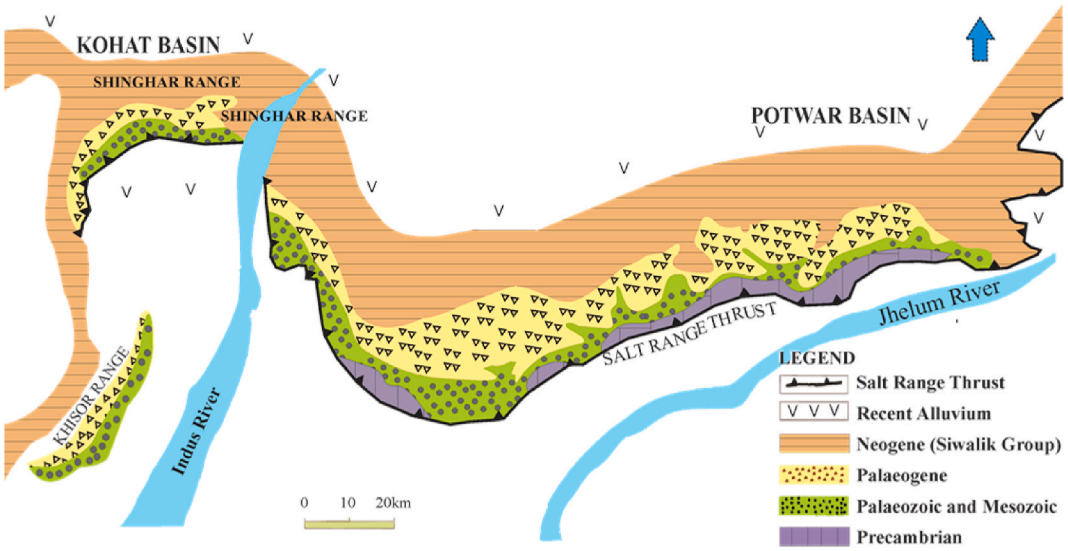


**Fig. 2.** Structural styles and regional tectonic setting of the Kohat-Potwar Plateau (modified after Khan et al., 2018).

widely distributed WF-LM Formation in the Sichuan Basin consists of a set of black shale, thin-bedded silty gray-black mudstone, subordinate gray to dark gray carbonate rocks, and gray to dark-gray siltstone. Like the Kohat-Potwar Plateau, Sichuan Basin is also affected by multiple stages of tectonic movements, forming a series of NE-SW echelon folds which contribute to the present-day tectonic framework (Liang et al., 2012; Zhang et al., 2017). Based on those similarities, we suppose that Patala formation in Pakistan, like WF-LM Formation in China, could be a potential shale gas play.

In this research, we establish an integrated approach by analyzing fundamental elastic and petrophysical rock properties, Rock-Eval pyrolysis, and sealing mechanism of roof and floor together to evaluate the shale gas prospects in Patala Formation. This research aims to first, identify the generative potential and thermal maturity by Rock-Eval pyrolysis. Secondly, estimate the characteristics of shale gas accumulation (TOC, porosity, thickness, and burial depth). Then, overlapping the extracted data on proposed brittleness templates to distinguish the brittle, ductile, and transitional zones and finally interpret the structural style and develop the sealing model of shale roof and floor for gas preservation.

## 2. Geological settings and stratigraphy

### 2.1. Geology and stratigraphy of the Kohat-Potwar Plateau Pakistan

There are two categories of sedimentary basins in Pakistan: (i) Indus Basin (ii) Baluchistan Basin. The Greater Indus Basin is categorized further into three sub-basins: the upper, middle, and lower Indus basins. Infracambrian to rocks of recent age (Quaternary) have been deposited in Indus Basin and also exposed on the surface (Meissner et al., 1974; Shah, 2009; Ahmed et al., 2019). Kohat-Potwar Geologic Province (also called Plateau in the literature), is a part of upper Indus Basin, located at the northern highlands of Pakistan (Fig. 1). It is limited by the Parachinar-Muree fault and Kala Chitta Range to the north, Kalabagh fault to the west, Jehlum fault to the east, and Salt Range thrust to the south. The surface field geological investigation and interpretation of the geophysical data indicate intense folding and thrusting, multiple salt-affected and basement involved uplifting due to transpressional tectonic evolution (Shah, 2009) (Fig. 1).

The river Indus divides the Kohat-Potwar Plateau into two parts: the eastern part is known as Potwar Plateau and the western part known as Kohat Plateau (Fig. 2). The Kohat-Potwar Plateau is one of the highly complex tectonic units of northern Pakistan due to the active ongoing collision between the Indian and Eurasian plates (Meissner et al., 1974; Ahmed et al., 2019). The structural map of the study area shows that the western part is tectonically more deformed compared to the eastern part (Fig. 2). A thick sequence of Infracambrian evaporates deposits started to infill the basin, covered by a thin succession of platform deposits from Cambrian to Eocene and thick molasse sediments from Miocene-Pliocene (Fatmi, 1973; Ali et al., 2009a, 2009b).

In Potwar Plateau the Infracambrian Salt Range provided main detachment from the Eocene-to-Cambrian (E-C) sequence as a consequence of intense tectonic activity (Ghazi et al., 2015, 2020). In addition, the E-C sequence resulted in numerous folds and faults for oil and gas traps due to the compressional forces (Ahmed, 2003). In the eastern Potwar Plateau, this sequence varies from less than 50 m to more than 400 m.

The Kohat Plateau, in the western part, is tectonically more complex with steeper dips (more than 30°) and typical asymmetrical structures associated with large-scale normal and reverse (thrust) faults (Khan et al., 2012). It is characterized by complex fold-fault patterns from Eocene to Pliocene, where salt of Eocene has occupied the cores of many anticlines (Pivnik and Wells, 1996). In this Plateau, a very thin deposition of sediments during most of the Cretaceous reveals emergence and erosion of land due to the fall of sea. This rise of land was more significant in the southern and eastern segment, as evident by less deposition in the lower and upper Cretaceous (Ahmed, 2003). Unfortunately, limited exploration activity and geological information about unconformities and major change in deposition leave Kohat Plateau poorly defined (Khan et al., 2012).

As regards petroleum system, the Kohat-Potwar Plateau is the oldest petroleum producing basin in Pakistan with first oil discovery dating back to 1914 (Shah, 2009; Khan et al., 2018). Kohat-Potwar Plateau reached a mature stage of oil window and several oil and gas fields have been discovered from different reservoir units (Cambrian to Paleocene-Eocene clastics and carbonates) (Fig. 1) (Nazir et al., 2020).

The study area's stratigraphic framework is established from the outcrop and drilled wells (Fig. 3a). This stratigraphic sequence shows that the deposition was interrupted several times resulting in non-deposition or unconformities that are schematically shown in Fig. 3a and discussed in the following subsections;

#### 2.1.1. Eocene-miocene unconformities

Non-orogenic movements comprising multiple uplifts of various cycles, affecting pre-Eocene deposition. Later in the Eocene, gradual withdrawal of the sea water caused the complete emergence of the area

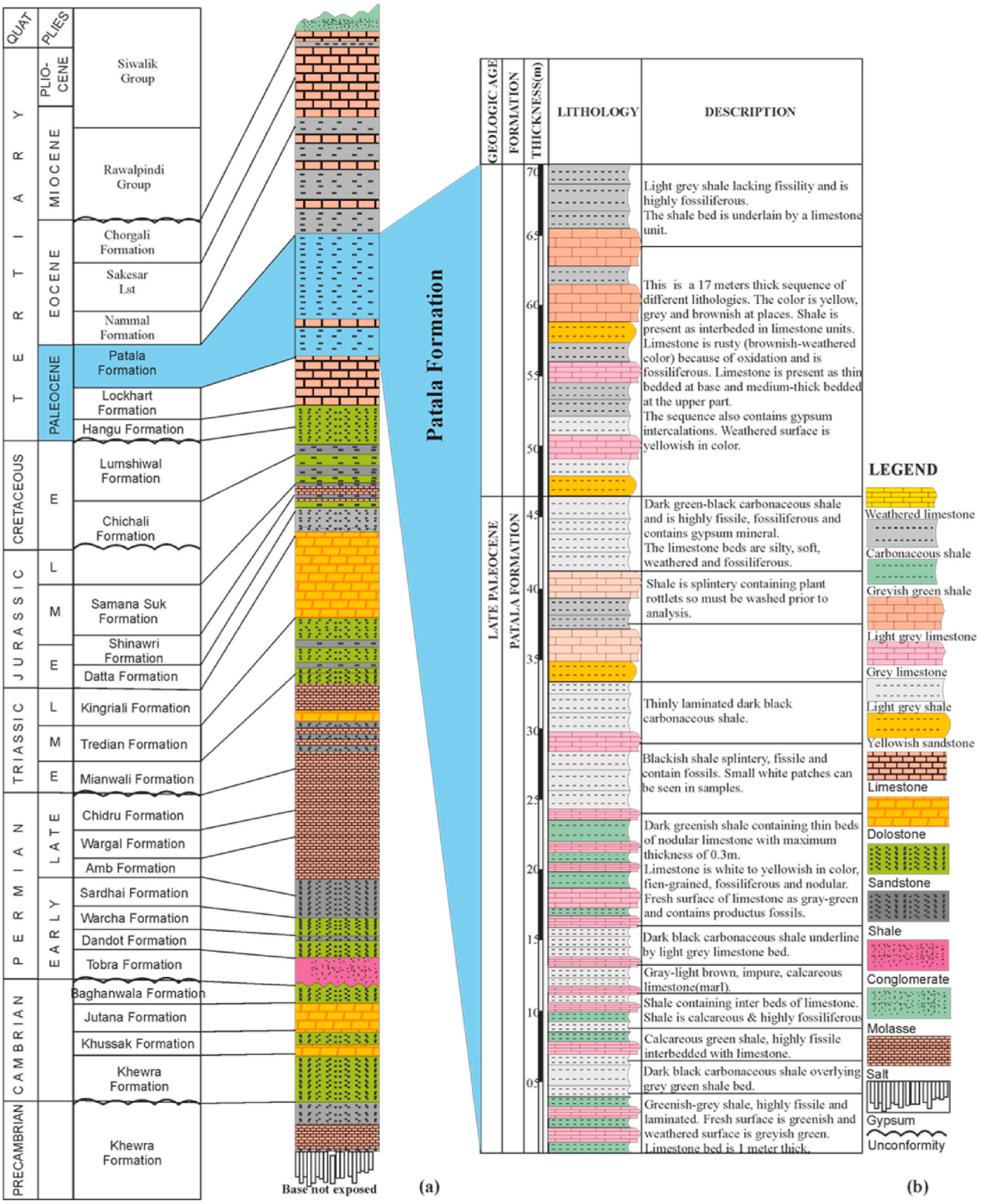


**Fig. 3.** (a) Generalized stratigraphic framework of the study area, (b) Field investigation of Patala Formation (modified after Fatmi, 1973; Khan et al., 2018).

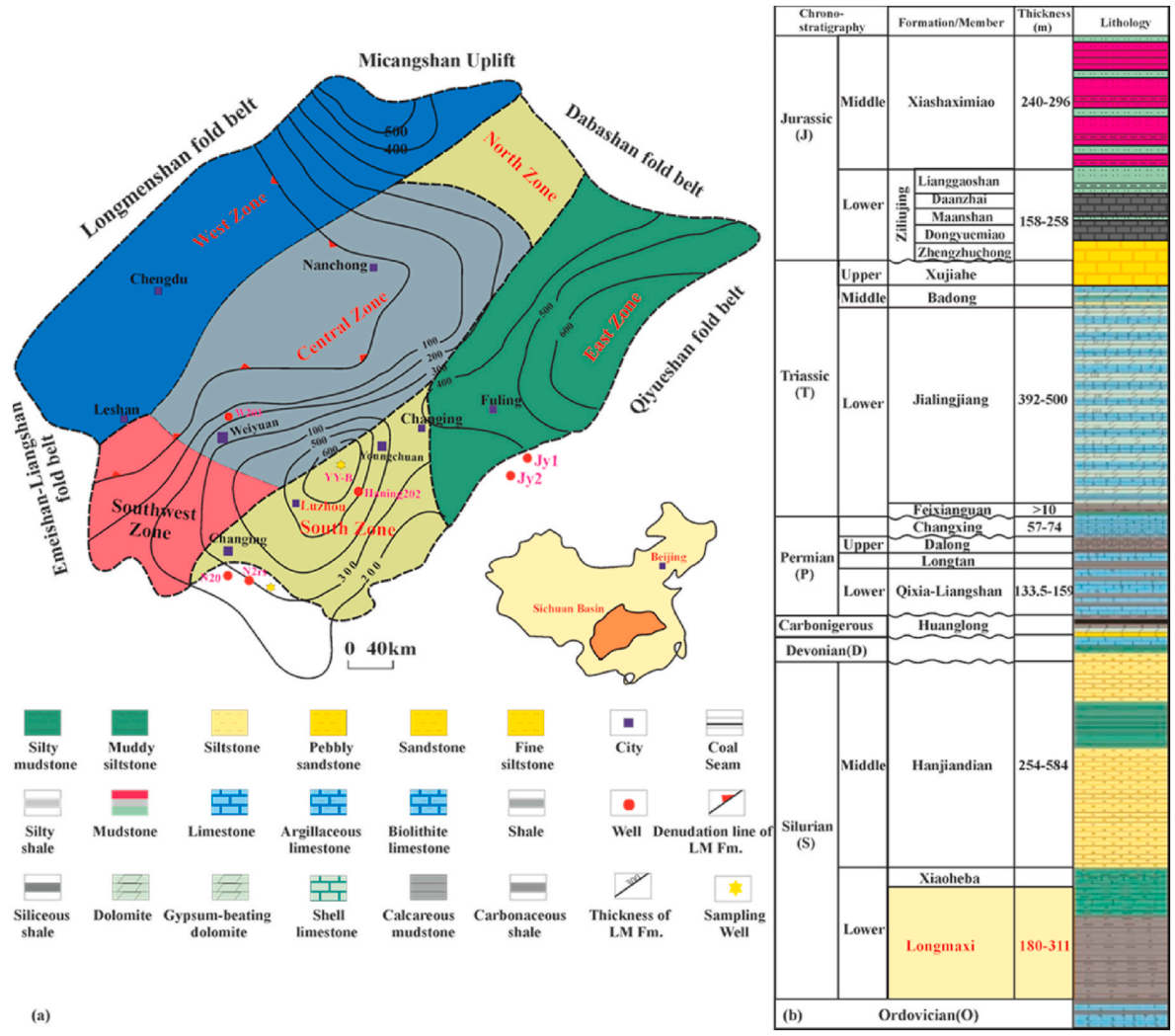


**Fig. 4.** (a) Generalized stratigraphic framework, (b) location of shale gas fields, the thickness of the WF-LM Formation, and tectonic units (represented with a different color) in the petroliferous Sichuan Basin China (modified after Dai et al., 2014). (For interpretation of the references to color in this figure legend, the reader is referred to the Web version of this article.)

(Shah, 2009).

#### 2.1.2. Cretaceous-paleocene unconformities

During the Cretaceous, most of the area emerged due to the regressive sea and contributed to erosion. In the southern and eastern part of the area, the emergence was most extreme, as indicated by the non-deposition of the Cretaceous section.

#### 2.1.3. Late jurassic-early cretaceous unconformities

By the late Jurassic, the land emerged from the sea resulting in a non-deposition and unconformity. Then, sedimentation started again during the Cretaceous.

### 2.2. Late paleocene Patala Formation

Shallow-marine late Paleocene Patala Formation is composed of thin-bedded marl and gypsum intercalations, medium- or thick-bedded carbonaceous (organic-rich) black and light gray shale, gray and white to light gray limestone, a minor fraction of greenish to yellowish-brown sandstone, and coal (Fig. 3b). The shale is highly fossiliferous and locally laminated. The limestone is rusty due to oxidation and fossiliferous, and occurs as inter-bedded with shale. The sandstone has fine to medium grain size and is deposited by medium-to thin-bedded (Khan et al., 2018). The Lockhart limestone underlies the Patala Formation with a transitional contact relationship (Fig. 3a). The Patala Formation is overlain by a transitional contact based on increase of limestone inter-beds of Eocene Nammal Formation comprising both limestone and shale (Shah et al., 1977). The estimated thickness of Patala Formation in the Kohat-Potwar Plateau, varies from 25 m to 140 m. However, maximum thickness about 182 m has been reported in the Hazara area (Khan et al., 2018).

Studies conducted by Wandrey et al. (2004), HDIP (Hydrocarbon development institute of Pakistan), and BGR (Bundesanstalt für Geowissenschaften und Rohstoffe Germany) on rock core samples revealed that the Patala Formation is the main hydrocarbon generating source for most of the reservoirs in Kohat-Potwar region. Previous studies by Fazeelat et al. (2010) and Wandrey et al. (2004) on Rock-Eval pyrolysis of Patala Formation suggest that it has sufficient source rock potential.

### 2.3. Geology and stratigraphy of the Sichuan Basin China

The petroliferous Sichuan Basin is located in the southwestern part of China with total areal coverage of approximately 5 × 104 $km^2$ and contains substantial reserves of shale gas (Liang et al., 2012). The basin is bounded by various fold belts and fault zones, including Longmenshan fault and fold belt in the West, Dabashan fold belt in the North,

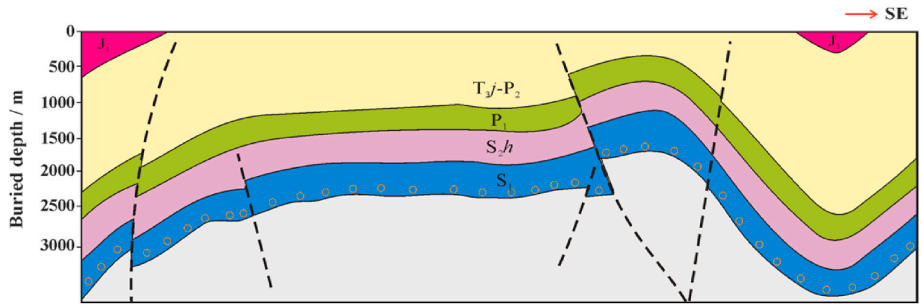


**Fig. 5.** Structural styles and regional tectonic setting of the Sichuan Basin China (modified after Tang et al., 2020).

Emeishan-Liangshan fold belt in the SW, and Qiyueshan fold belt in the East (Fig. 4a).

The basin emerged from a Sinian-Middle Triassic (Z1-T2) passive continental margin resulting in deposition of thick marine carbonates and clastics interbedded with layers of volcanic rocks (Fig. 4b). The Sichuan Basin was deformed by the closure of the Palaeotethys and the oceanic sub-duction of the Yangtze platform during the Late Triassic (Huang et al., 2012; Liang et al., 2016). During the Jurassic-Quaternary period, it was primarily a foreland basin stage which resulted in uplift, folding, and erosion. The region was affected by multiple stages of tectonic movements, forming a series of NE-SW echelon folds which contribute to the present-day tectonic framework (Huang et al., 2012; Liang et al., 2012, 2016) (Fig. 5).

Dating back to the late Ordovician, the various uplifts which supplied low-energy formed a confined sea providing deep-water anoxic conditions (Huang et al., 2012; Liang et al., 2016). Afterward, the third period of the global transgression occurred at Ordovician-Early Silurian caused by the ice cap. Due to this transgression and multiple tectonic movement, a series of fine-grained clastic sedimentary rocks to primarily black shale were deposited. This occurred during the depositional stage of the early Silurian-age, LM Formation.

A thick sedimentary fill in the Sichuan basin is present from the Sinian-Middle Triassic to the Quaternary system (Fig. 4b). The Sinian-Middle Triassic system is mainly composed of 4100 m–7000 m thick marine sedimentary strata. In contrast, the upper Triassic-Quaternary system is composed of continental strata with a total thickness of 3500 m–6000 m. The Lower Paleozoic is divided into; (a) Lower Cambrian shale that was deposited in marine environment of deep-water shelf, (b) carbonates of Middle Cambrian Ordovician platform, and (c) Lower Silurian LM Formation that was deposited in shallow-marine environments during the Rhuddanian and Aeronian stages of the Silurian system (Li et al., 2016).

There are mainly two sedimentary cycles in the LM Formation, containing a set of black shale, gray-black (silty) mudstone, subordinate gray to dark gray carbonate rocks, and gray to dark-gray siltstone. The depositional setting of the black shale in the LM Formation is similar to that of the Middle East and North Africa shales as both were deposited through regional flooding during the early Silurian period (Liang et al., 2012; Dai et al., 2014; Soua, 2014). Rich carbonaceous rocks with good TOC and a significant amount of pyrite are present at the bottom of the LM Formation with a maximum thickness in the southern part of the Sichuan Basin. Anoxic deep-water shelf setting provided suitable environmental conditions to the black shale for the preservation of organic matter. The organic-rich LM Formation mostly contains sapropelic type

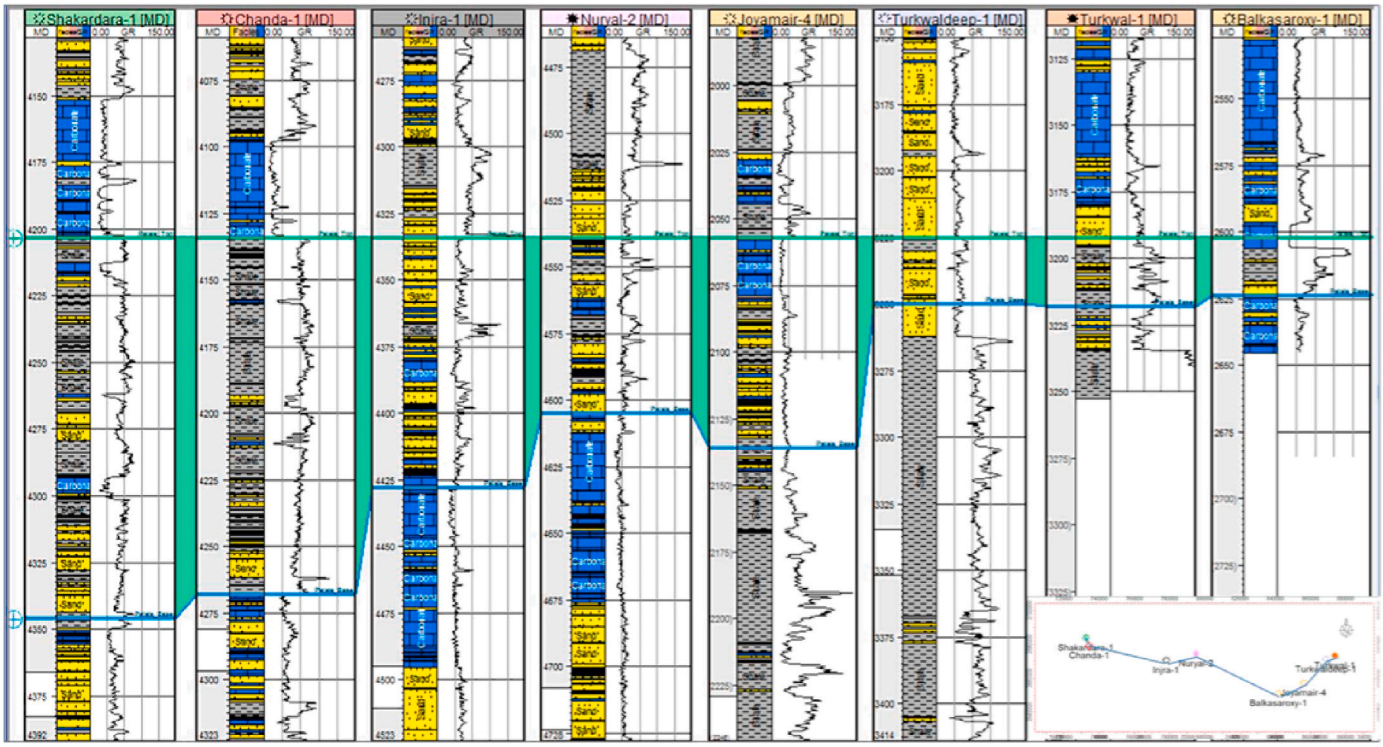


**Fig. 6.** Well correlation and subsurface stratigraphic analysis in the Kohat-Potwar Plateau. The top of the Patala Formation is flattened.

**Table 1**
Rock–Eval pyrolysis for Patala shale in the all eight wells.

| Well Samples | Lithology | $S_1$ | $S_2$ | $S_3$ | HI | OI | PI | Tmax (°C) | TOC (wt. %) |
|---|---|---|---|---|---|---|---|---|---|
| JM-01 | Limestone | 0.23 | 1.81 | 0.34 | 106 | 20 | 0.11 | 424 | 1.77 |
| JM-02 | Shale | 0.09 | 1.15 | 0.05 | 122 | 04 | 0.07 | 430 | 0.96 |
| JM-03 | Limestone | 3.29 | 19.5 | 0.18 | 201 | 02 | 0.14 | 445 | 9.88 |
| JM-04 | Limestone | 0.15 | 1.30 | 0.41 | 117 | 37 | 0.11 | 442 | 1.12 |
| NR-01 | Shale | 0.17 | 1.01 | 2.06 | 103 | 192 | 0.13 | 428 | 1.09 |
| NR-02 | Shale | 0.42 | 1.83 | 1.90 | 171 | 184 | 0.19 | 422 | 1.05 |
| NR-03 | Shale | 0.16 | 1.02 | 2.01 | 84 | 158 | 0.11 | 428 | 1.32 |
| NR-04 | Shale | 0.32 | 1.98 | 2.14 | 173 | 205 | 0.14 | 424 | 1.08 |
| NR-05 | Shale | 1.81 | 3.40 | 2.02 | 312 | 202 | 0.20 | 420 | 1.06 |
| NR-06 | Shale | 0.27 | 1.21 | 1.99 | 74 | 117 | 0.16 | 424 | 1.74 |
| NR-07 | Shale | 0.52 | 1.83 | 1.96 | 84 | 94 | 0.22 | 428 | 2.16 |
| SK-01 | Shale | 0.16 | 1.19 | 1.71 | 145 | 212 | 0.11 | 432 | 0.80 |
| SK-02 | Shale | 0.42 | 1.28 | 1.64 | 173 | 242 | 0.14 | 438 | 0.71 |
| SK-03 | Shale | 0.11 | 1.00 | 1.82 | 152 | 276 | 0.12 | 434 | 0.66 |
| SK-04 | Shale | 0.27 | 1.51 | 2.16 | 83 | 121 | 0.13 | 430 | 1.80 |
| SK-05 | Shale | 0.12 | 1.43 | 1.05 | 161 | 114 | 0.11 | 434 | 0.92 |
| SK-06 | Shale | 0.16 | 1.92 | 1.16 | 173 | 108 | 0.07 | 434 | 1.14 |
| BK-01 | Limestone | 0.52 | 20.98 | 1.34 | 253 | 17 | 0.04 | 428 | 8.20 |
| BK-02 | Shale | 0.51 | 1.60 | 0.07 | 192 | 80 | 0.20 | 422 | 0.88 |
| BK-03 | Shale | 0.37 | 5.61 | 1.64 | 183 | 55 | 0.03 | 428 | 3.00 |
| TKD-01 | Shale | 0.12 | 1.43 | 1.07 | 97 | 72 | 0.10 | 434 | 1.48 |
| TKD-02 | Shale | 0.56 | 1.82 | 1.21 | 184 | 138 | 0.21 | 416 | 0.94 |
| TKD-03 | Shale | 0.42 | 1.18 | 1.04 | 143 | 135 | 0.24 | 424 | 0.76 |
| TK-01 | Limestone | 0.81 | 16.40 | 1.82 | 302 | 34 | 0.05 | 428 | 5.45 |
| TK-02 | Shale | 0.12 | 3.98 | 0.64 | 113 | 25 | 0.04 | 426 | 2.80 |
| TK-03 | Shale | 0.21 | 1.40 | 2.22 | 102 | 202 | 0.20 | 404 | 1.13 |

and mixed oil and gas hydrocarbons (Type I and Type II) (Dai et al., 2014).

## 3. Materials and methods

### 3.1. Data description

Borehole logs data from eight exploratory wells: Balkassaroxy-1, Turkwal-1. Turkwaldeep-1, Joyamair-4, Injra-1, Nuryal-2, Chanda-1 and Shakardara-1 (Fig. 1), were used for estimating the TOC, porosity, mineralogy, kerogen volume, dynamic Young's modulus and Poisson's ratio in Patala Formation. In addition, twenty six well cuttings were obtained from those wells at regular intervals of the Patala Formation to measure the mineralogical composition, Rock-Eval pyrolysis and TOC content. In the present study, we utilized 1000 km of 2D seismic data to mark the stratigraphic horizons and structural style, focusing particularly on the sealing capacities of the roof and floor strata for gas preservation in the Patala Formation.

The gamma-ray log curves from all the eight wells were used to construct a subsurface cross-section along the correlation line extending from east (Potwar Plateau) to west (Kohat Plateau) (as shown to the right side of Fig. 6). The sedimentary succession in all eight wells have encountered shale, limestone, sandstone, and dolomite. According to the cross-sectional analysis, Patala Formation shows significant thickness variation increasing from the eastern to the western part of the study area (Fig. 6).

### 3.2. TOC analysis

#### 3.2.1. Laboratory analyses (Rock-Eval pyrolysis)

The maturity and generative potential of Patala Formation was determined from Rock-Eval parameters, such as oxygen index (OI), production index (PI), hydrogen index (HI), and maximum temperature (Tmax). The details of Rock-Eval pyrolysis parameters are presented in the abbreviation list at the end of the paper. Vinci Rock-Eval 6 apparatus was used by following the procedures reported previously (Tissot and Welte, 1984; Waples, 1985; Espitalié et al., 1985; Peters and Cassa, 1994). Approximately twenty six well cuttings samples were investigated to measure the OI, HI, TOC, PI, and Tmax, as shown in Table 1. TOC content of the twenty six samples, collected from well cuttings of the Patala Formation, was determined on a LECO's CS230-series carbon and sulfur determinator by following the formal standards process (CNS GB/T19145-2003).

#### 3.2.2. Log-based TOC estimation

In addition to laboratory based TOC analysis, the ΔLOGR technique of Passey et al. (1990) (which estimates TOC content on the basis of apparent difference between the porosity log and resistivity) and Schmoker methods (Schmoker and Hester, 1983) were selected (because no heavy minerals like pyrite was present in Patala Formation) to evaluate TOC from well logs.

The modified Schmoker method for calculating TOC is shown as follows (Jiang et al., 2018):

$$Schmoker_A = \frac{1}{1 - \frac{1}{\rho_g}} \tag{1}$$

$$Schmoker_B = Schmoker_A - 1 \tag{2}$$

$$TOC_{Schmoker} = \frac{Schmoker_A}{\rho_b} - Schmoker_B \tag{3}$$

where $\rho_g$ is grain density and $\rho_b$ is bulk density log.

The ΔLOGR technique was established by Passey et al. (1990). The technique involves an overlaying of properly scaled porosity and deep resistivity curves to observe the deviation in log response values due to the influence of organic matter.

$$TOC_{\Delta LOGR} = \Delta LOGR_{Sonic} \times 10^{(2.297-(0.169\times LOM))} \tag{4}$$

To calculate the $\Delta LOGR_{Sonic}$ and $LOM$, the following equations (5) and (6) are used:

$$\Delta LOGR_{Sonic} = \log\left[\frac{R_{LLD}}{R_{LLD\_baseline}}\right] + 0.02 \times \left[DTP_{Sonic} - DTP_{Sonic\_baseline}\right] \tag{5}$$

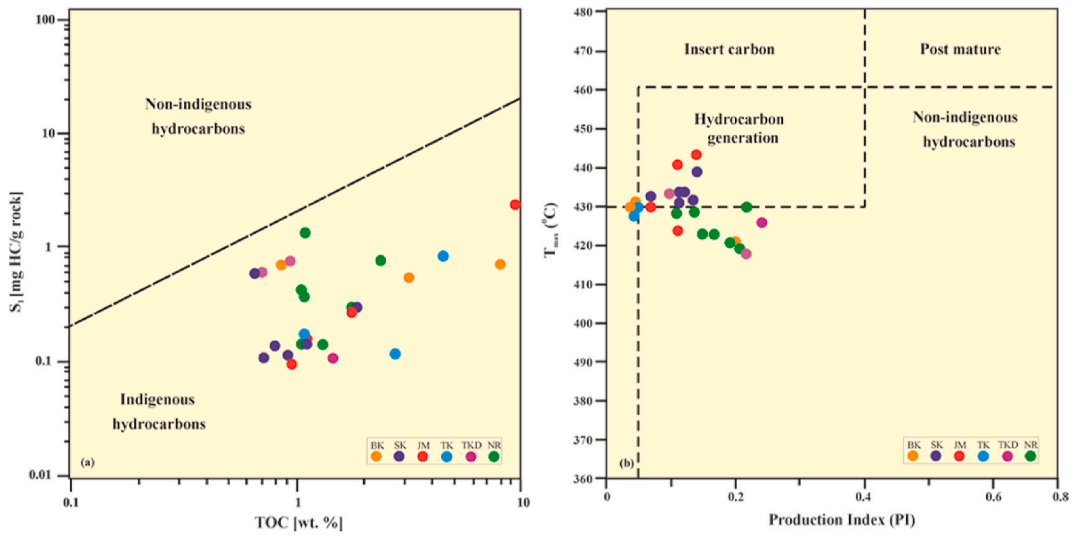


**Fig. 7.** (a) Cross plot of $S_1$ versus TOC to differentiate between indigenous and non-indigenous hydrocarbons (after Fakhri et al., 2013), (b) generative potential of the Patala Formations in studied wells (after Shalaby et al., 2012).

$R_{LLD\_baseline} = 6\ \Omega$ m.
$DTP_{Sonic\_baseline} = 295\ \times$ μsec/m

$$LOM = 0.099 \times x^5 - 2.159 \times x^4 + 12.39 \times x^3 - 29.03 \times x^2 + 32.53 \times x^1 - 3.034 \quad (6)$$

where *LOM* is called level of maturity and *x* is vitrinite reflectance = 0.93 taken from Ali et al. (2017).

The average of TOC $\left(\frac{TOC_{schmoker}+TOC_{\Delta LOGR}}{2}\right)$ estimated by both ΔLOGR and Schmoker methods will be compared with the TOC content measured from Rock-Eval pyrolysis to estimate the TOC of Patala Formation in all eight wells.

### 3.3. Porosity

In the literature (Katz et al., 1995; Crain and Holgate, 2014; Zhu et al., 2018), the porosity in shale zone is usually estimated by a single 'porosity log' (sonic, density, neutron), within deep resistivity log. However, better estimation of porosity is possible with the combination of neutron and sonic logs because we can make some very useful inferences about lithology and fluid content (Sohail and Hawkes, 2020; Yasin et al., 2020a). The total corrected porosity (based on the combination of neutron and sonic logs, as shown in equation (9)) is used to estimate porosity of Patala Formation in all eight wells. The details of total porosity obtained from the combination of neutron and sonic logs are described by Sohail and Hawkes (2020) in the following equations (7)–(9):

$$\varnothing_{eff\_sonic} = \varnothing_{sonic} - V_{TOC} \times \varnothing_{TOC} - V_{cl} \times \varnothing_{cl} \quad (7)$$

$$\varnothing_{eff\_neutron} = NPHI - V_{TOC} \times \varnothing_{TOC} - V_{cl} \times \varnothing_{cl} \quad (8)$$

$$PHIT_{corrected} = \varnothing_{eff} = \frac{\varnothing_{eff\_sonic} + \varnothing_{eff\_neutron}}{2} \quad (9)$$

where $\varnothing_{cl}$ and $V_{cl}$ are porosity and volume of clay respectively. In equations (7) and (8), $\varnothing_{cl}$ is the clay porosity in the shaly interval (with maximum GR value). $V_{TOC}$ is volume of TOC and NPHI is the neutron porosity log to measure porosity directly. $\varnothing_{TOC} = 0.53$ and 0.65 for sonic log and neutron log-based porosities, respectively.

### 3.4. Kerogen volume

Researchers proposed various log-based models to calculate the kerogen volume in shale intervals using the bulk density of non-organic matter (Shazly et al., 2013). The mass-balance model (Vernik et al., 1997), as given in equation (10), is deemed more suitable for shale gas reservoirs and used for the estimation of kerogen volume in Patala Formation:

$$V_{kerogen} = \frac{TOC}{C_k} \times \frac{\rho_b - \rho_f \varnothing}{\rho_k (1 - \varnothing)} \quad (10)$$

where $V_{kerogen}$ is kerogen volume and $C_k$ is maturity level (0.7–0.85), $\varphi$ is porosity, $\rho_b$ is bulk density, $\rho_k$ is kerogen density and $\rho_f$ is fluid density, i.e., 0.5 g/cm$^3$ was taken for Patala Formation.

### 3.5. Dynamic Young's modulus and Poisson's ratio

In this study, the values of typical dynamic Young's modulus and Poisson's ratio for Patala Formation were calculated from equations (11) and (12) (Mavko et al., 2009; Yasin et al., 2020b):

$$E_{dynamic} = \frac{\rho_b \times V_s^2 \left(3V_p^2 - 4V_s^2\right)}{\left(V_p^2 - V_s^2\right)} \quad (11)$$

$$\nu_{dynamic} = \frac{V_p^2 - 2V_s^2}{2\left(V_p^2 - V_s^2\right)} \quad (12)$$

where $E_{dynamic}$ represent dynamic Young's modulus and $\nu_{dynamic}$ for Poisson's ratio, $\rho_b$ is bulk density of formation, and compressional and shear wave velocities are represented by *Vp* and *Vs*, respectively.

## 4. Results and discussions

### 4.1. Computation of TOC

The measured TOC values in Patala Formation show high net organic richness, ranging from 0.66 to 9.88 (wt. %). About 70% of the samples contain more than 1 wt% of TOC (Table 1). These values indicate that the Patala Formation could be a good source rock and may also be reservoir rocks (shale gas reservoir). Well cuttings from dark black color carbonaceous (organic-rich) layers in Patala Formation are rich in

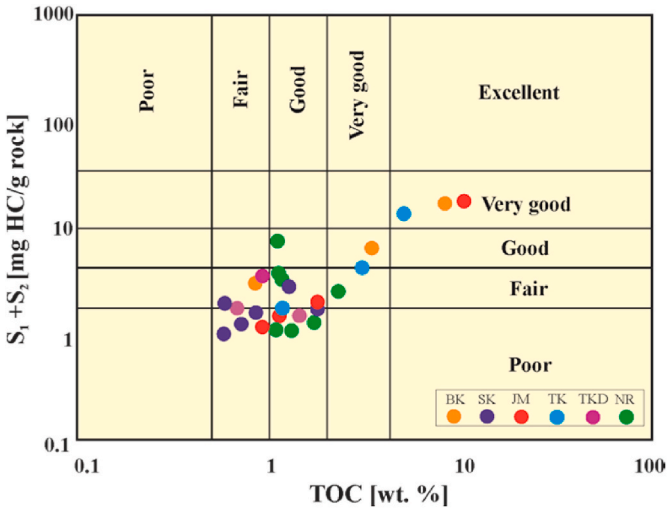


**Fig. 8.** $S_1$+$S_2$ pyrolysis versus TOC plot determining the petroleum-generative potential and qualitative assessment of yield of Patala Formation (modified after Ghori and Haines, 2007).

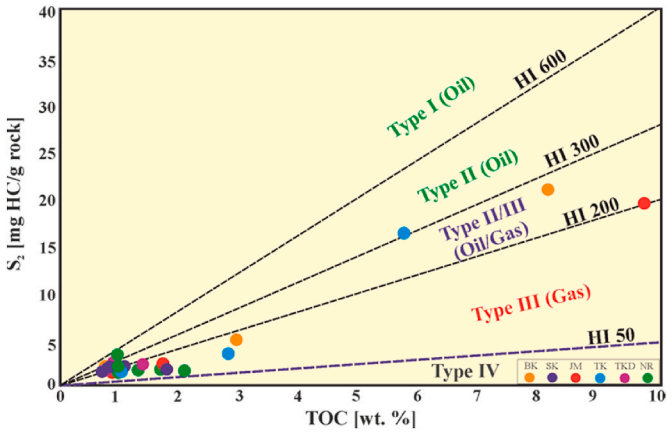


**Fig. 9.** $S_2$ pyrolysis versus TOC plot to investigate kerogen types in the Patala Formation (modified after Peters et al., 2006).

organic matter and have excellent TOC content. In contrast, those taken from the thin dark gray carbonaceous layers indicate moderate-to-good TOC content (Fig. 3). These carbonaceous dark black and gray layers in Patala Formation determine then a moderate-to-good potential of shale gas. The comparison of TOC results with the measured TOC in Longmaxi shale reports that both shales have similar reservoir quality with complex multi-phase tectonic history (Tang et al., 2019). However, TOC content solely predicts shale gas potential and cannot evaluate the production of hydrocarbon. Therefore, it should be combined with Rock-Eval pyrolysis results to analyze the generative potential of the Patala Formation (Makky et al., 2014).

### 4.2. Rock-Eval pyrolysis

Rock-Eval pyrolysis results from cuttings samples in the eight wells indicate good amount of the free hydrocarbons ($S_1$) yield ranging from values of 0.09 mg/g to 3.94 mg/g with an average of 0.54 mg/g (Table 1). Likewise, $S_2$, i.e., thermally cracked hydrocarbons yield range from 1.01 mg/g to 20.98 mg/g with an average of 2.06 mg/g (Table 1). Both the amounts of hydrocarbons ($S_1$ and $S_2$) indicate promising results, i.e., fair-to-good and very good hydrocarbon generative potential.

The cross plot of $S_1$ versus TOC shows that the hydrocarbons of analyzed samples of Patala Formation in the studied wells are mainly

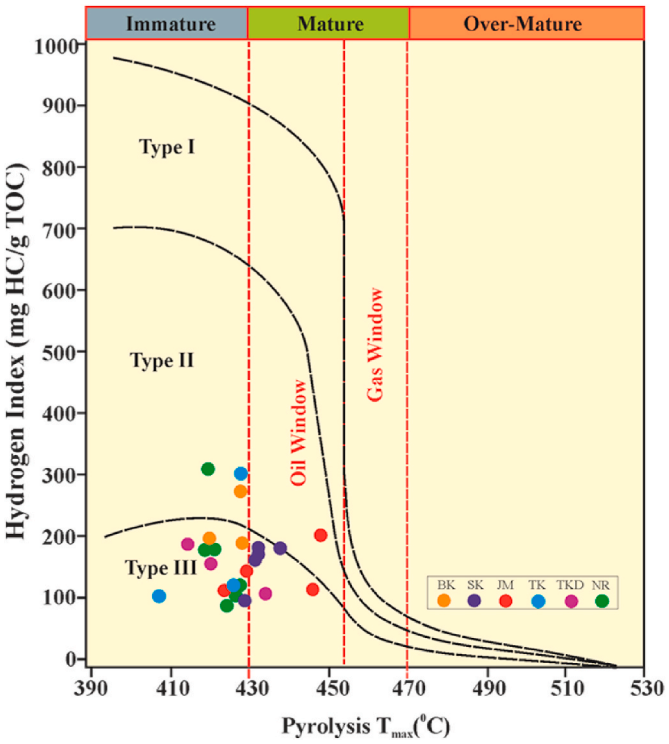


**Fig. 10.** Rock-Eval hydrogen index (HI) versus $T_{max}$ plot, indicating kerogen types and thermal maturation stages in Patala Formation (modified after Peters, 1986 and Hunt, 1996).

indigenous to the source rock (Fig. 7a). The cross plot between TOC and $S_1$ usually differentiates the indigenous and non-indigenous hydrocarbons and have been discussed in detail by Hunt (1996), Fakhri et al. (2013), and Abd-Allah et al. (2018) and (2019). Also, the cross plot of $T_{max}$ versus PI indicates that majority of samples in Patala Formation attained the hydrocarbon generation stage as $T_{max} > 430$ °C while only few samples fall on the margin of hydrocarbon generation stage (Fig. 7b).

#### 4.2.1. Generative potential of Patala Formation

The hydrocarbon generative potential of Patala Formation is further evaluated using $S_1$+$S_2$ pyrolysis versus TOC (wt. %) graph as proposed by Hunt (1996) and shown in Fig. 8. Plotting the data on a graph of $S_1$+$S_2$ pyrolysis versus TOC indicates fair-to-good and very good hydrocarbon generative potential in Patala Formation.

Plotting the data from HI, TOC, and $S_2$ in bivariate standard kerogen plots indicates various hydrocarbon-generative types in the Patala Formation (Fig. 9) suggesting predominantly both type II/III kerogen (both gas prone and oil prone) and type III kerogen (mainly gas-prone organic matter).

#### 4.2.2. Thermal maturity and hydrocarbon generation

Thermal maturity in Patala Formation is assessed by plotting $T_{max}$ (°C) against HI (mg HC/g of TOC) (Fig. 10). In Table 1, $T_{max}$ ranges from 416 °C to 445 °C with an average value of 430, and HI varies from 74 mg HC/g to 312 mg HC/g with an average of 187 mg HC/g. Fig. 10 shows that the carbonaceous dark green and black shale layers of the Patala Formation reached the early stage of maturation (thermally immature) to mature stage and can generate sufficient hydrocarbons. Mashhadi et al. (2015) and Abdel-Fattah et al. (2017) reported that the thermal maturity level of organic matter is affected by burial depth and types of organic matter. Thus, we investigated the burial-history of the Patala Formation to interpret this marginal maturation result.

The burial-history plot indicates that the initial burial began at about

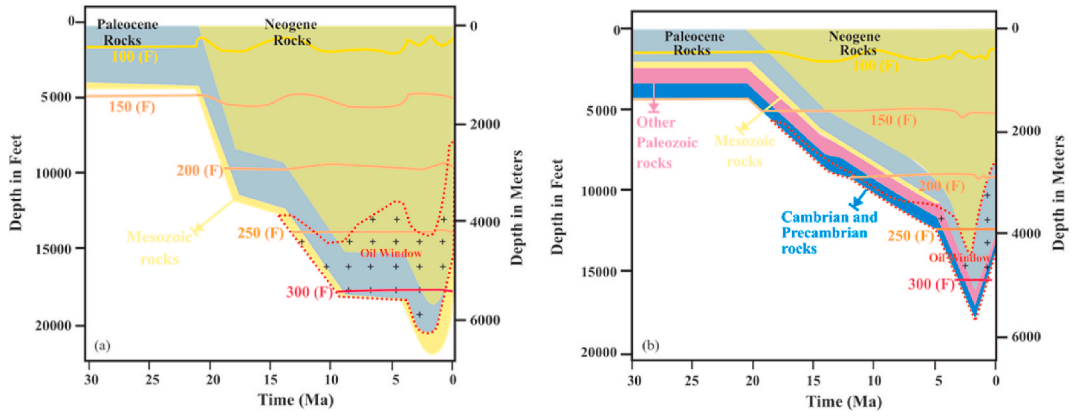


**Fig. 11.** Generalized burial-history plots, (a) Kohat Plateau, (b) Potwar Plateau.

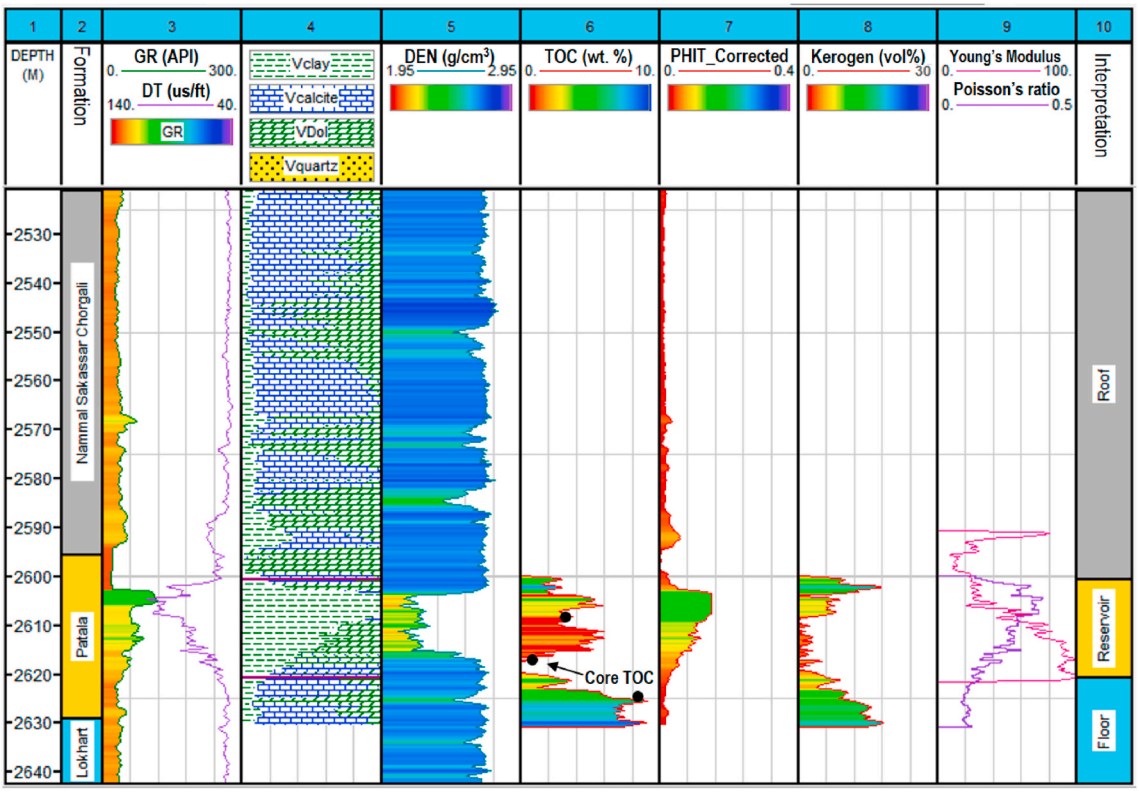


**Fig. 12.** Interpretation of petrophysical properties in Balkassaroxy-1 well of Potwar Plateau.

30 Ma and has continued to the present (Fig. 11). The period of hydrocarbon generation was started about 20 to 15 Ma. The burial-history plots from the two wells of the Kohat-Potwar Plateau indicate that maximum burial was reached nearly 2 million years ago. The plots also show that the onset of the oil window (0.60–1.1% $R_o$) of the Paleocene rocks (Patala Formation) attained the early stage of maturation to mature stage and still in the oil window (Fig. 11a and b). Law et al. (1998) reported two distinct overpressuring regimes, (a) Neogene, (b) pre-Neogene. Both regimes were attributed to tectonic compression and undercompaction and hydrocarbon generation was started during pre-Neogene.

### 4.3. Petrophysical characterization

#### 4.3.1. Patala Formation in the Kohat-Potwar Plateau

The bulk mineralogy of Patala Formation was estimated using conventional logging tools, such as formation density, deep resistivity, neutron porosity, compressional and shear sonic, gamma-ray, and photoelectric absorption. The dominant mineral component is clay, calcite, and dolomite with minor amounts of quartz, and unidentifiable feldspar and pyrite minerals (Fig. 12, track 4). This mineralogical composition is consistent with the previous study conducted by Jalees and Tahira (2020) on the rock core samples (thin sections) of Patala Formation.

The TOC content and kerogen volume in Patala Formation ranges from 0 to 8.5 (wt. %) and 5 to 20 (vol. %), respectively, as shown in Fig. 12 (tracks 6 and 8). The average TOC curve (estimated from ΔLOGR and Schmoker methods) compares favorably with laboratory-measured TOC. Note that the kerogen volume increases with increasing TOC content.

The average porosity from the combination of the neutron-sonic formula with clay corrected gives better results and ranges from 0% to

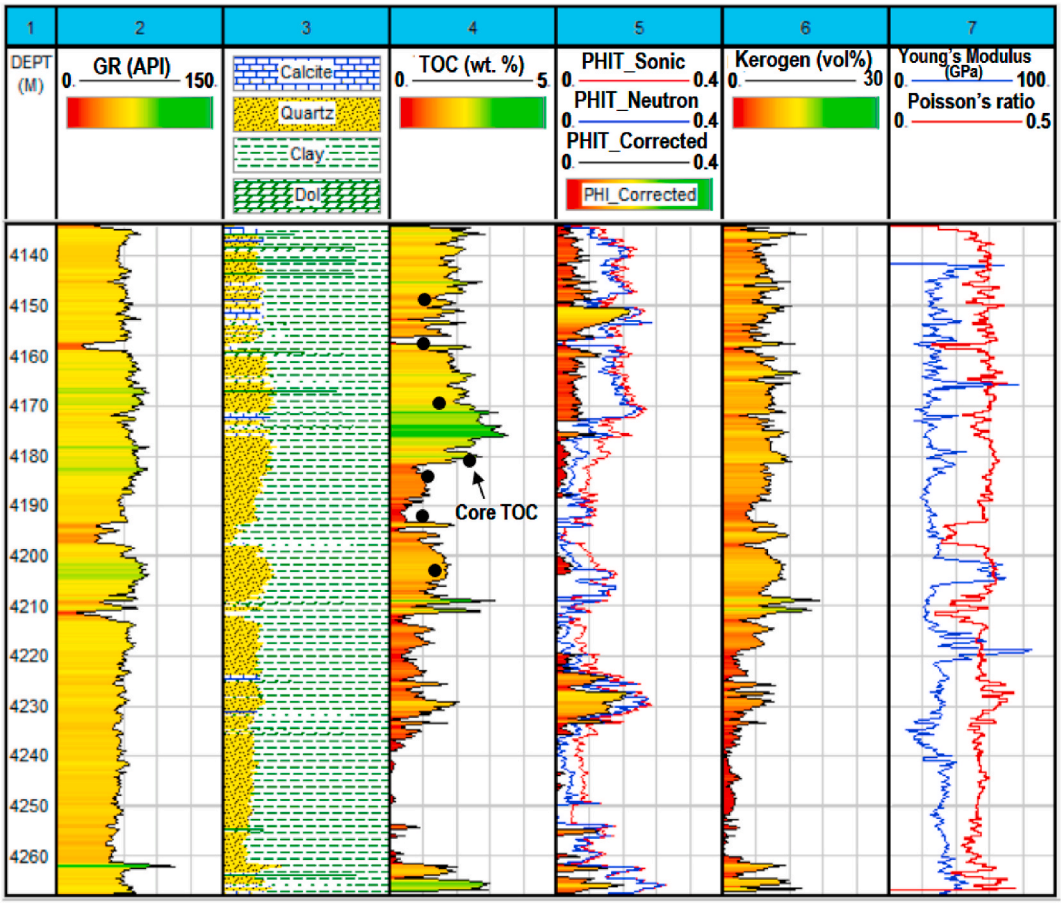


**Fig. 13.** Interpretation of petrophysical properties of Patala Formation in Nuryal-2 well of Kohat Plateau.

14% (Fig. 12, track 7).

The density of the Patala Formation is low compared to the Nammal-Sakassar-Chorgali, and Lokhart Formations, which can act as the roof and floor of the Patala Formation, respectively (Fig. 12, track 5).

The dynamic Young's modulus varies between 10 GPa (minimum) to 80 GPa (maximum) throughout the interval, except two distinct zones of very high values (~100 GPa). The dynamic Poisson's ratio also fluctuates from 0.1 to maximum 0.4. Both Young's modulus and Poisson's ratio show highly variable character, i.e., Young's modulus is high when Poisson's ratio is low, throughout the Patala shale interval (Fig. 12, track 9).

The petrophysical properties of Patala Formation in Nuryal-2 well of Kohat Plateau are not similar to those in Balkassaroxy-1 well of Potwar Plateau (Fig. 13). The dominant mineral component in Nuryal-2 well are clay and quartz with minor amounts of calcite and dolomite. The TOC content and kerogen volume in Nuryal-2 well are low and ranges from 0 to 2.5 (wt. %) and 2 to 12 (vol. %), respectively (Fig. 13, tracks 4 and 6). However, the average TOC curve shows good close-match with laboratory-measured TOC.

#### 4.3.2. *Wufeng-longmaxi formation in the Sichuan Basin*

Since the Patala Formation in the Kohat-Potwar Plateau Pakistan has similar structural styles and multiphase tectonic setting with the proven Longmaxi shale gas in Sichuan Basin China, we suggest to investigate the petrophysical parameters of this WF-LM Formation. Logs data from vertical well are used to estimate the petrophysical parameters in WF-LM shale gas reservoirs. In WF-LM Formation the TOC content varies from 0.2 to 5.6 wt %, with an average of 2.2 wt % (Fig. 14, track 2). The TOC content changes with the lithology and the highest values occur in laminated siliceous to argillaceous shale but gradually decrease due to increasing quartz content (Liang et al., 2012, 2016). The high amounts of TOC indicate good adsorption capacity of WF-LM shale gas with free gas (methane) content varying from 0.5 to 6.0 $m^3/t$ approximately (Fig. 14, track 7).

The reservoir properties vary from poor to medium range, e.g., porosity ranging from a minimum of 3.77% to maximum of 8.7% with an average of about 6.2%. WF-LM Formation exhibit very low permeability values, ranging from 0.005 mD to a maximum of 0.012 mD with an average value of about 0.0116 mD (Liang et al., 2016). Laboratory analysis as well as the results of log data interpretation of WF-LM Formation indicate that the lithology is dominated by quartz and clay minerals throughout the vertical section. Other minerals in descending order of mineral content are calcite, dolomite, and pyrite (Fig. 14, track 6).

The water saturation ($S_W$) and density of WF-LM member (LM1~1) is low as compared to the upper WF-LM member (LM1~2 and LM1~3) and lower WF-LM member (LX) which are acting as good roof and floor for the WF-LM Formation, respectively (Fig. 14, track 3, 4).

### 4.4. *Shale gas reservoir characteristics*

#### 4.4.1. *Thickness and TOC distribution*

The thickness and organic richness of the Patala Formation in Kohat-Potwar Plateau are highly variable and show different character from one region to another. The maximum thickness of Patala Formation in Kohat Plateau is up to145 m but in Potwar Plateau it varies between 45 and 75 m (Fig. 15). The lateral variation in the thickness of Patala Formation changes sharply from west (Kohat Plateau) to the east (Potwar Plateau). Even though the overall depositional environment during the late Paleocene was open marine, various cycles of uplifting may have

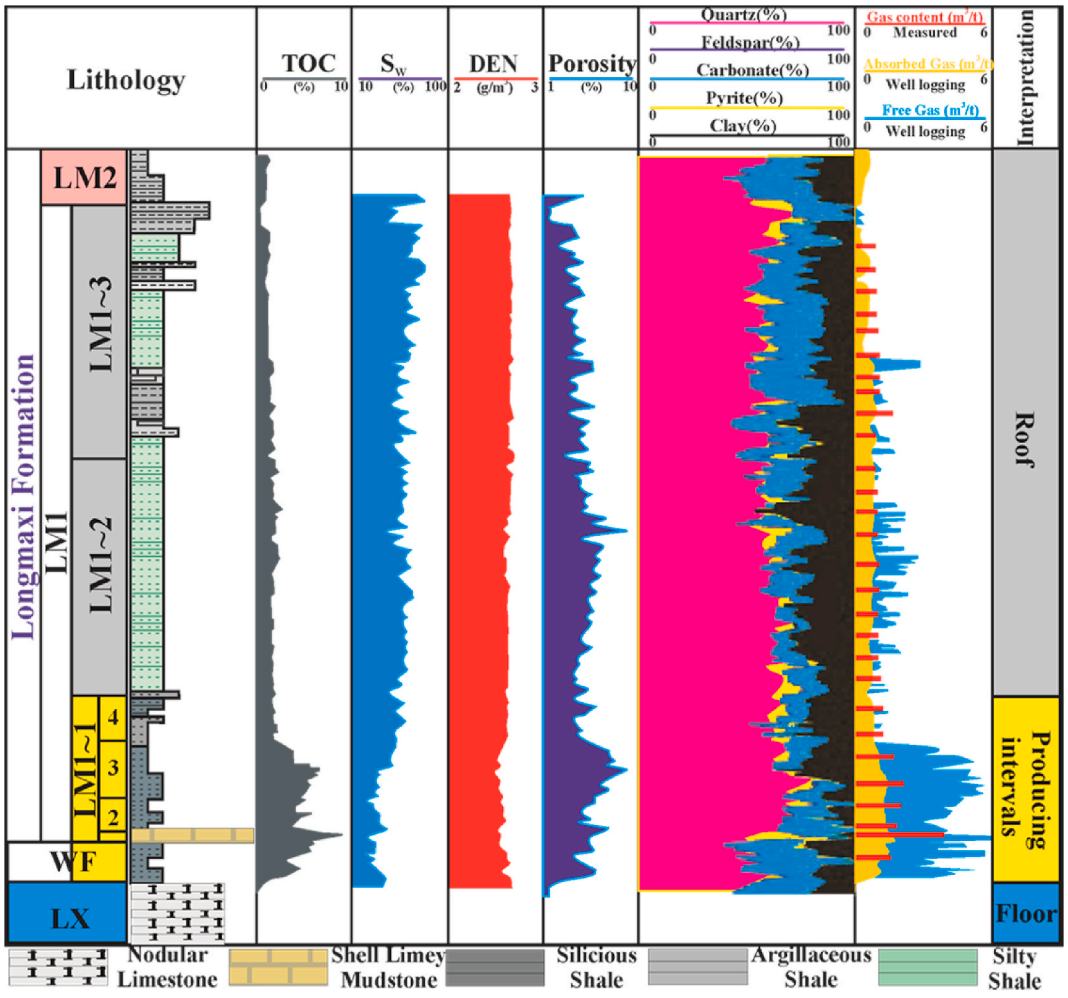


**Fig. 14.** Interpretation of petrophysical properties in shale gas well of WF-LM Formation.

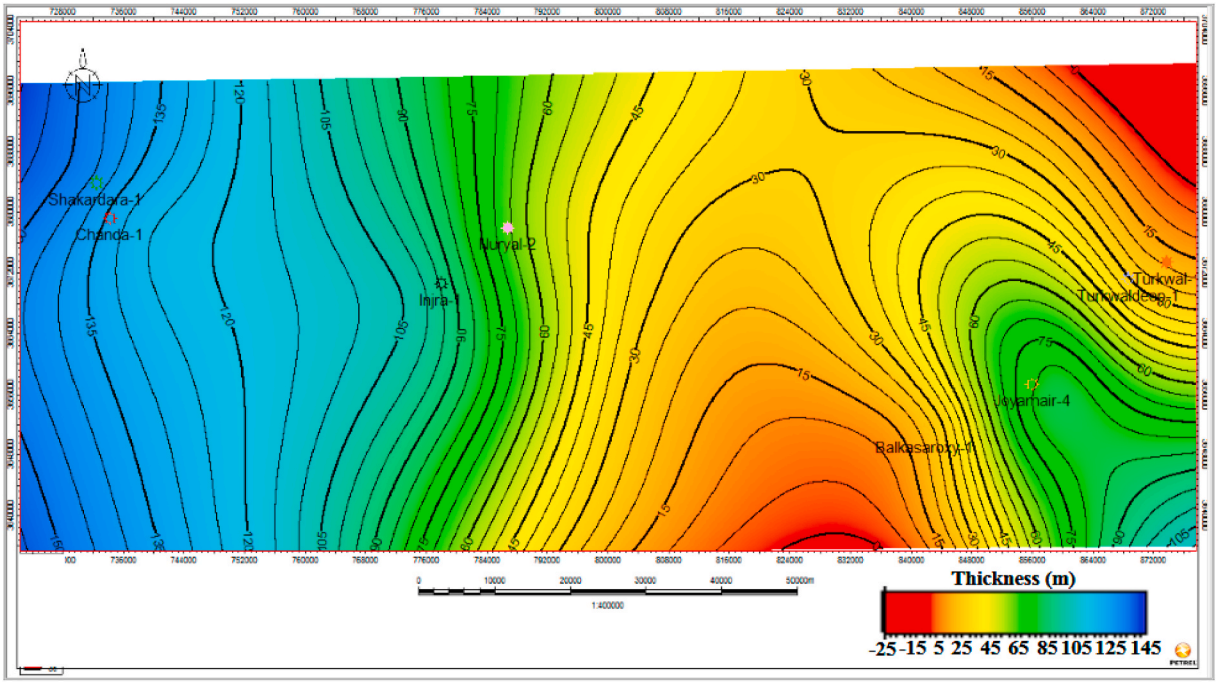


**Fig. 15.** The lateral thickness map of Patala Formation in the Kohat-Potwar Plateau.

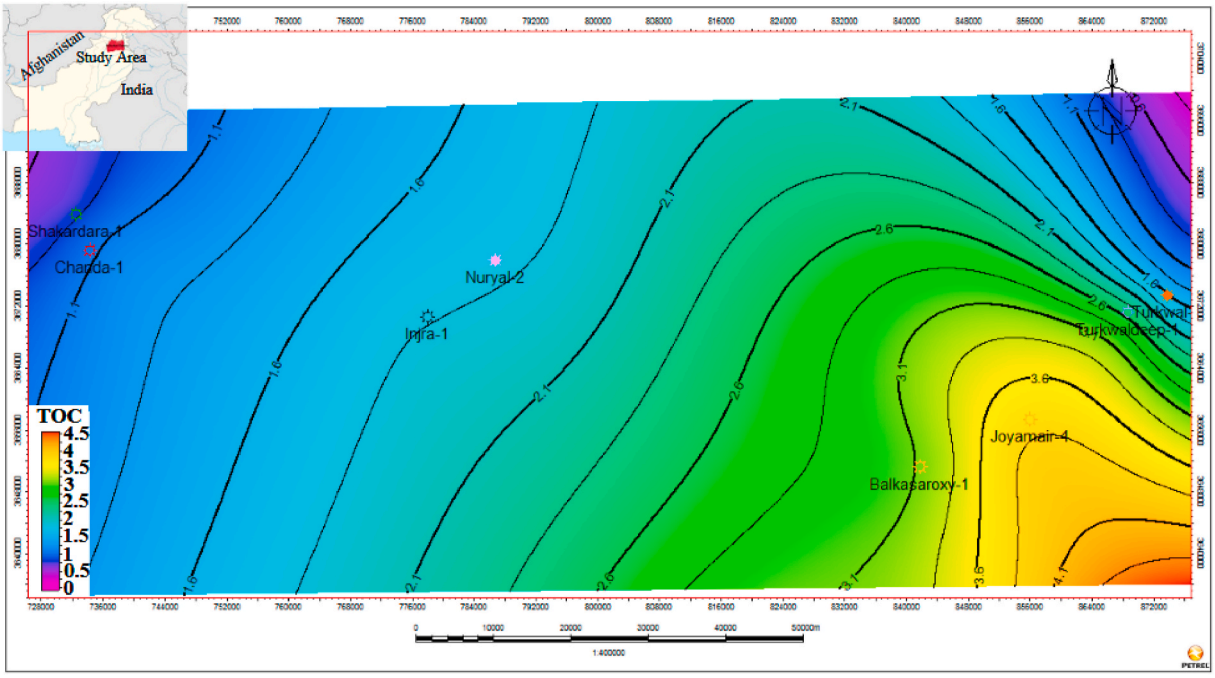


**Fig. 16.** The TOC distribution map in the Kohat-Potwar Plateau.

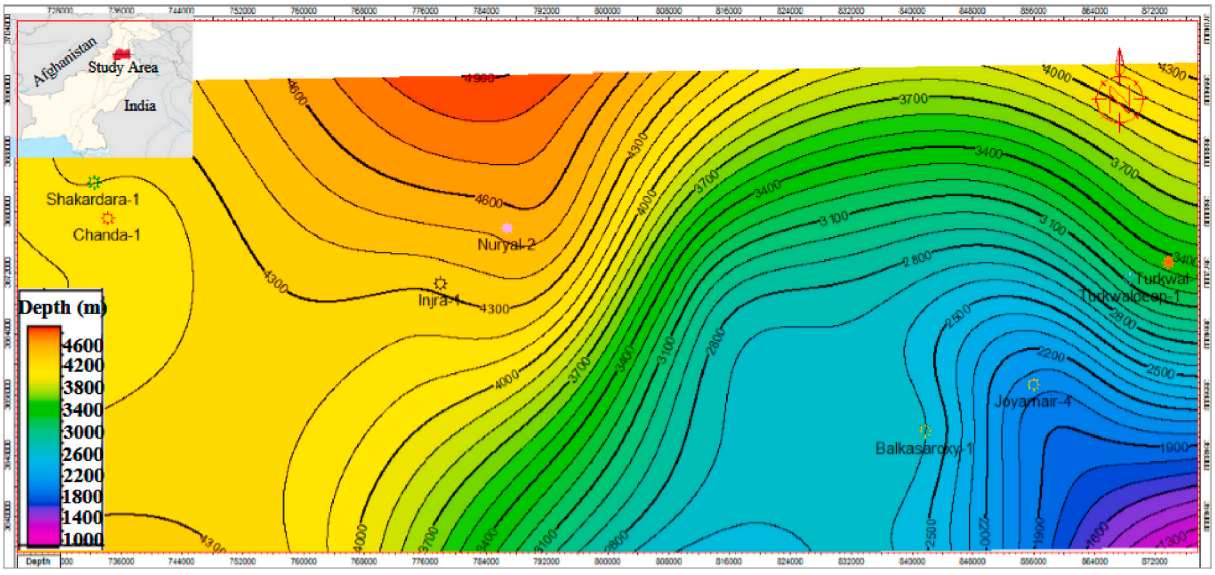


**Fig. 17.** The depth contour map of Patala Formation in the Kohat-Potwar Plateau.

affected the deposition in the Kohat and Potwar Plateau (Meissner et al., 1974; Ahmed, 2003; Ahmed et al., 2019).

The organic content in the Kohat-Potwar Plateau also varies within a single basin. The highest TOC content is found in the Potwar Plateau and gradually decreases to the western part in Kohat Plateau (Fig. 16). Note that the TOC content and thickness here show inverse pattern with each other. For example, the thickness of Patala Formation in Joyamair-4 (Potwar Plateau) is 75 m with a TOC of 3.1 (wt. %), however, on the western side, in Chanda-1 (Kohat Plateau) Patala Formation has thicker strata of 135 m but TOC ranges from 1.1 to 2 (wt. %) only (Fig. 16). It is worth mentioning that the thickness of the source rock has, actually, no relation to hydrocarbon generation potential. The hydrocarbon generation depends mainly on TOC, maturity, enough maturity from depth of burial and thermal concerns, and reservoir petrophysical parameters associated with source rock. That is why we suggest thereafter investigating the burial depth, porosity, and mineralogy.

### 4.4.2. *Burial depth*

In the Kohat and Potwar Plateau, the burial depth varies from less than 2400 m to more than 4500 m, (Fig. 17). The gradual increases in burial depth from Potwar Plateau (east) to Kohat Plateau (west) indicate steeper dip due to multiple uplifting events. It should be noted that the Patala Formation with burial depth less than 2400 m has thickness >30 m and TOC >2 (wt. %). This seems to be logical that increasing burial depth undergoes increase in temperature, and then the source rock will be matured. As being more and more mature, the rock will generate and expel hydrocarbons resulting in the consumption of the reactive organic matter and so decrease in TOC content. This could explain why Patala

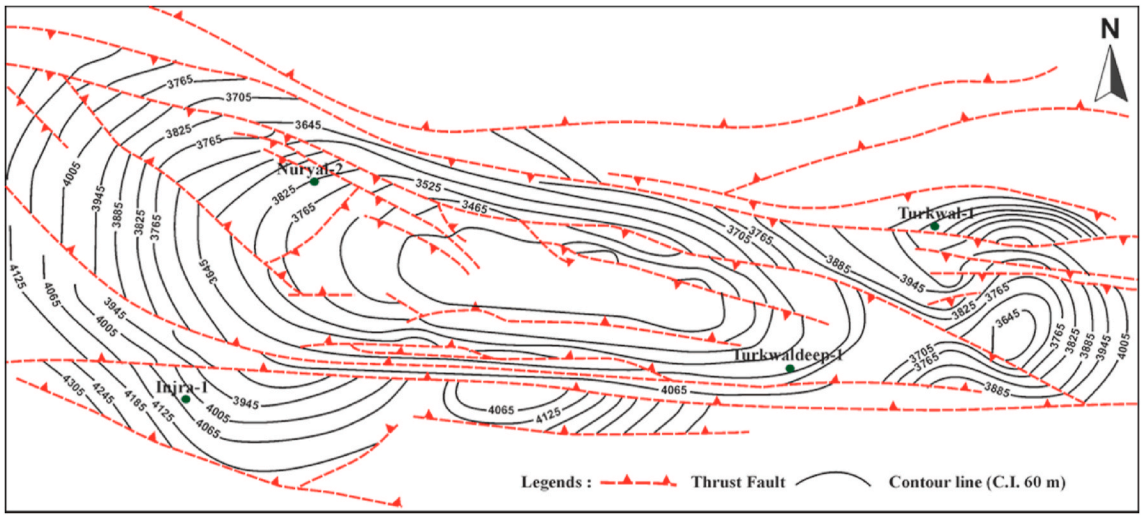


**Fig. 18.** Seismic structure contour map on the top of Paleocene rocks in the Kohat-Potwar Plateau.

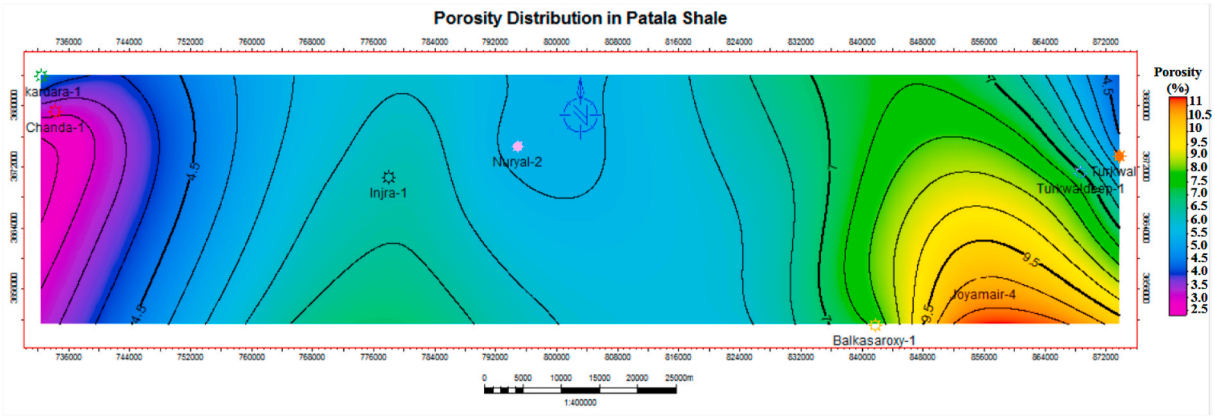


**Fig. 19.** The lateral distribution of porosity map in the Kohat-Potwar Plateau.

Formation in Potwar Plateau with shallow burial depth has high TOC content regardless to its small thickness comparing to Kohat Plateau. Also, lithological variations and direction of deposition could be the main factors controlling the variation in organic matter richness in Kohat-Potwar Plateau. Actually, the depositional conditions in Potwar Plateau is more deltaic as compare to Kohat Plateau.

Furthermore, the seismic structure map on the top of the Paleocene rocks (Patala Formation) shows east-west structural trend with pop-up, salt cored, plunging, and gentle dipping anticline restricted by thrusts in the north and south (Fig. 18). The seismic structure map, on its side, shows also that the burial depth increases gradually from east to west where the anticline moved upward along the fault surfaces and formed a

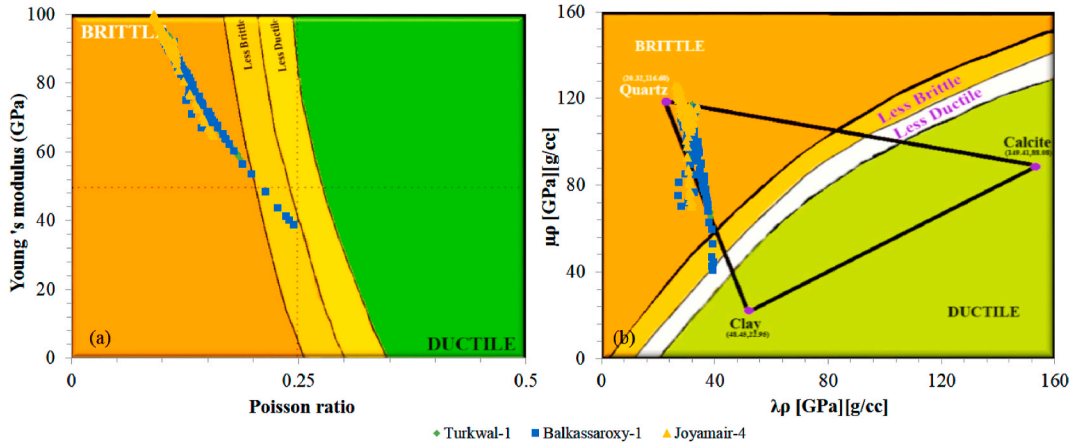


**Fig. 20.** The cross-plot of elastic parameters, (a) Young's modulus versus Poisson's ratio, (b) λρ versus μρ in Potwar Plateau. Note that the cross-plots are over-lapped to the proposed brittleness templates (Yasin et al., 2018), corresponding to Patala Formation in the three key wells from Potwar Plateau.

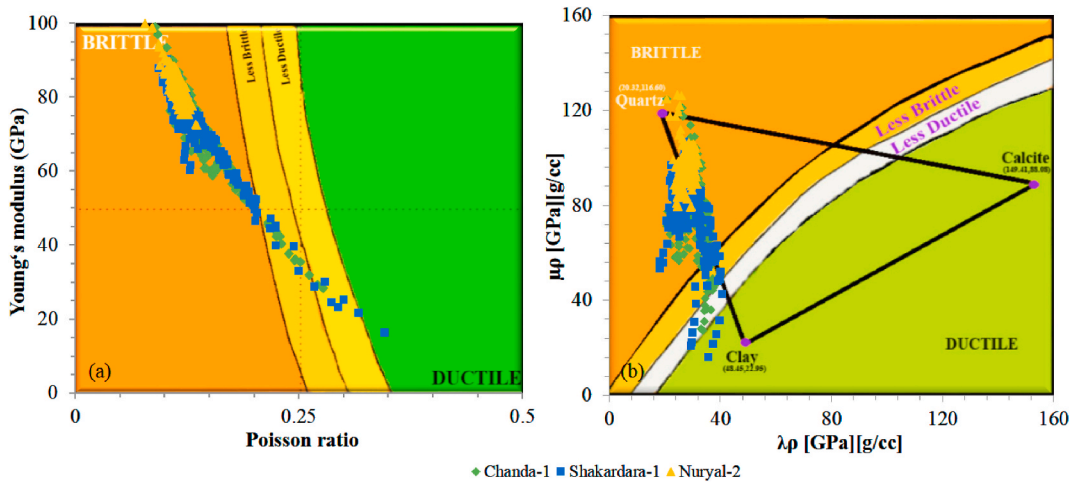


**Fig. 21.** The cross-plot of elastic parameters, (a) Young's modulus versus Poisson's ratio, (b) λρ versus μρ in Kohat Plateau. Note that the cross-plots are over-lapped to proposed brittleness templates (Yasin et al., 2018), corresponding to Patala Formation in the three key wells from Kohat Plateau.

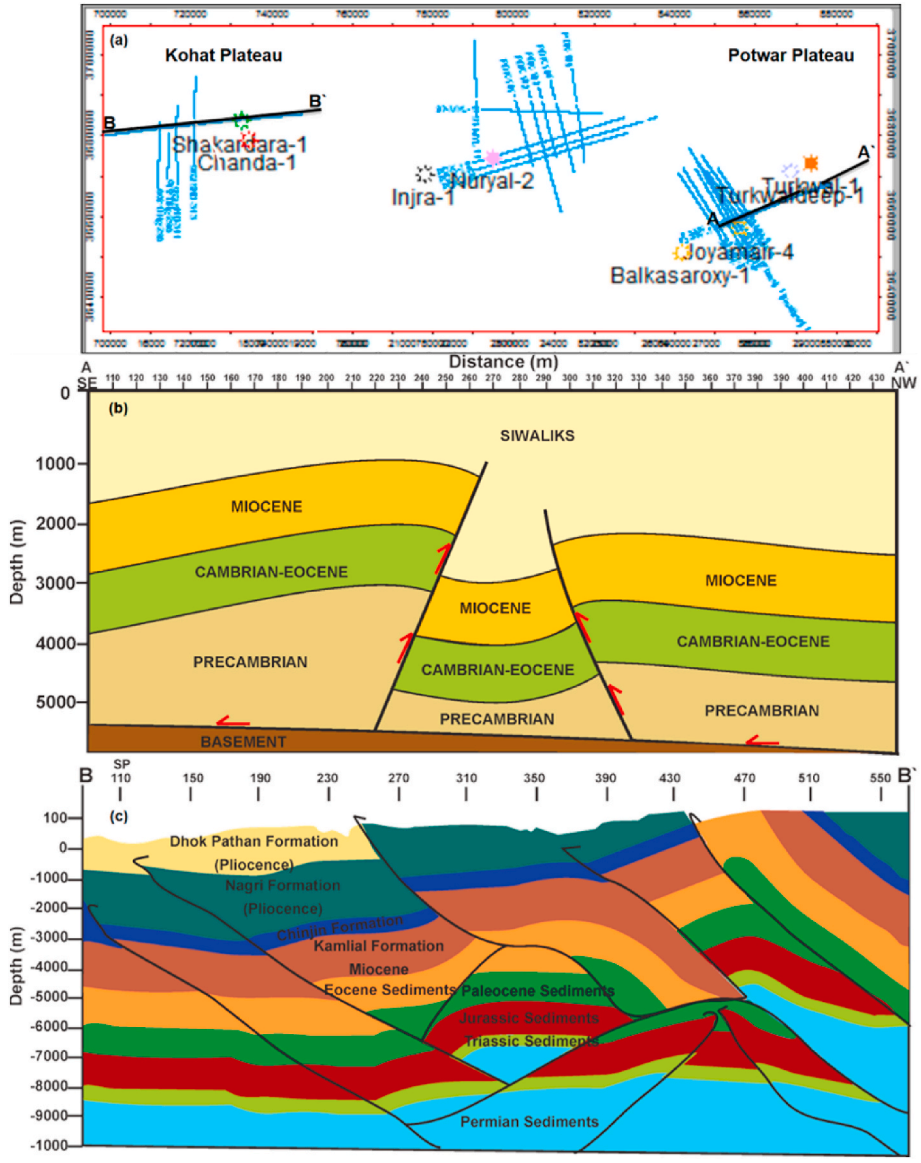


**Fig. 22.** The interpreted geo-seismic sections, (a) seismic lines base map of Kohat-Potwar Plateau, (b) seismic cross-section along seismic line A-À (Potwar Plateau), (c) seismic cross-section along seismic line B–B' (Kohat Plateau).

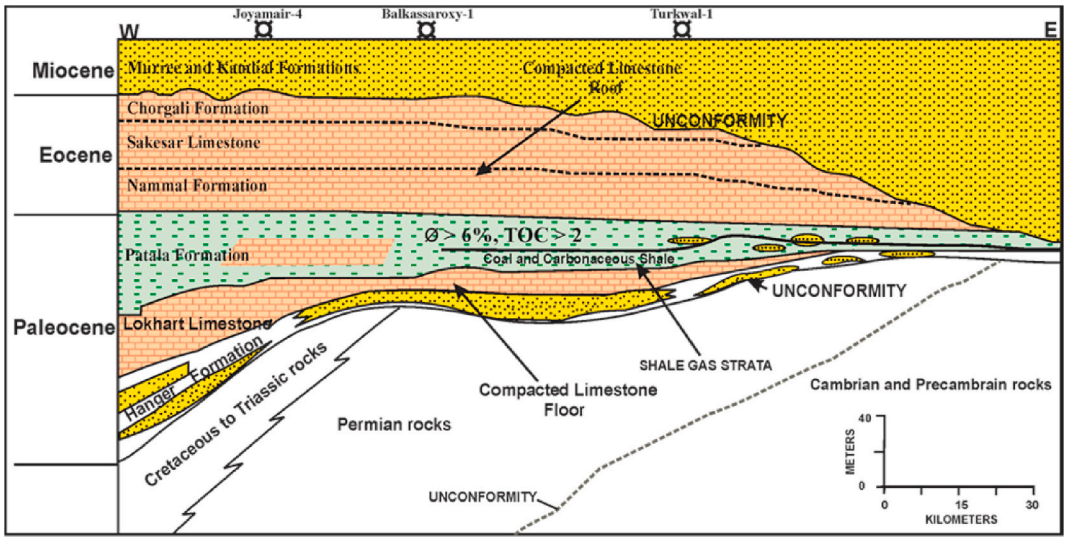


**Fig. 23.** Geological cross-section illustrating the roof and floor of the Patala Formation (modified after Warwick and Shakoor, 1993).

pop-up structure in the east and west.

#### 4.4.3. Porosity

In shale gas reservoirs, the estimation of total porosity is challenging due to presence of platy clay minerals, fine-grained texture, and nanometer pores (Tang et al., 2020). The lateral distribution of porosity, derived from the neutron-sonic combination (equation (9)), from geostatistical modeling in Patala Formation shows good porosity ranging in the region, from 2% (Kohat Plateau) to 10% (Potwar Plateau), as shown in Fig. 19. It is notable that the region with TOC >2 (wt. %) and thickness >30 m at burial depth <2500 m has porosity ranges from 6 to 10%. The shallower the formation, the less compaction it would undergo, resulting in high porosity.

#### 4.4.4. Brittleness evaluation

In order to evaluate the brittleness in the Patala Formation, we used data from the six key wells: Turkwal-1, Balkassaroxy-1, and Joyamair-4 from Potwar Plateau and Chanda-1, Shakardara-1, and Nuryal-2 from Kohat Plateau. The aim was to extract Poisson's ratio, Young's modulus, λ (bulk modulus), μ (shear modulus), and ρ (density) values along the vertical section and overlap them to the brittleness templates proposed by Yasin et al. (2018).

The cross-plots of multiple elastic parameters, i.e., Young's modulus versus Poisson's ratio (Fig. 20a) and λρ (product of bulk modulus and density) versus μρ (product of shear modulus and density) (Fig. 20b) show that the majority of data points are strictly enclosed within the defined brittle region. Very few data points tend to fall into the less brittle region (transitional zone) to the proposed brittleness templates.

Furthermore, the cross-plots of Young's modulus versus Poisson's ratio (Fig. 21a) and λρ versus μρ (Fig. 21b) in the key wells from Kohat Plateau indicates also a brittle zone with few marginal points.

The overlaying of the extracted data on the proposed brittleness templates in all the key wells from Kohat-Potwar Plateau confirms the high brittle zones in Patala Formation. Also, good matching of Young's modulus versus Poisson's ratio and λρ versus μρ with TOC content and porosity increases the reliability for classifying the possible failure features of the rock mass and reservoir characterization of shale.

### 4.5. Factors controlling shale gas accumulation

#### 4.5.1. Structure style

After evaluating shale reservoir quality, the identification of structural styles is crucial for shale gas enrichment and high productivity (Guo and Ping, 2015). The most common structural styles in the world's basins consist in broad anticlines, synclines, folds, reverse and thrust faults, monoclines, fault-blocks and reefs. Normal structures like uplifts and anticlines are most favorable for shale gas preservation and enrichment than monoclines or fault-blocks. In anticlinal structures, breached anticlines are more effective than the anticlines with single fault (Aamir and Siddiqui, 2006). However, the single fault anticlines are more favorable for the storage and preservation of shale gas than double fault anticlines. In larger syncline structures, the double-edge fault-propagation anticlines are better than the single fault anticlines or plunging anticlines. In monocline structures, an overlying uniformity with monocline will be more promising than continuous strata sequence (Guo, 2013; Tang et al., 2020).

The structural style in Kohat-Potwar Plateau is interpreted through geo-seismic depth section along the two key seismic sections of A-À (Potwar Plateau) and B–B' (Kohat Plateau) (Fig. 22a). Seismic sections of A-A′ show two major blind thrusts originated from the basal detachment layer (Fig. 22b). The first major thrust occurs in the SE part of the section that cuts the Cambrian to Eocene Carapace and the Miocene up to the Siwaliks. Another blind back-thrust exists to the north of the triangle zone. The arrangement of structures shows that the fore-thrust is verging SE and back-thrust NW and forming a triangle zone.

In the seismic sections of B–B′, the pop-up and triangle zones are presented (Fig. 22c). The faults thrusted the Eocene over the Miocene and Pliocene rocks, like an imbricate stack cut through the seismic section potentially from the basal detachment to the surface. These faults are thrusted over the Nagri Formation on the hanging wall and Dhok-Pathan Formation (Pliocene) on the foot wall.

#### 4.5.2. Sealing mechanisms of the roof and floor

Guo (2013) observed that the overlying (roof) and underlying (floor) strata of shale reservoirs are significant for the accumulation of gas, as both provide good enclosures for shale gas enrichment in complex structural systems. Zagorski et al. (2012) reported that the roof and floor strata of Marcellus and Barnet shale gas fields are both tight limestone and significant for forming and preserving overpressure. They also claimed that shale gas enrichment is constrained by ten key parameters including: 1) abundance of organic matter, 2) maturity, 3) brittle mineral content, 4) clay mineralogy, 5) water saturation, 6) porosity, 7) permeability, 8) gas content, 9) large thickness, and 10) preservation conditions. In addition to these basic parameters, Zagorski et al. (2012) included formation pressure and tectonic settings for the shale gas assessments in the Marcellus shale gas exploration conditions. Likewise,

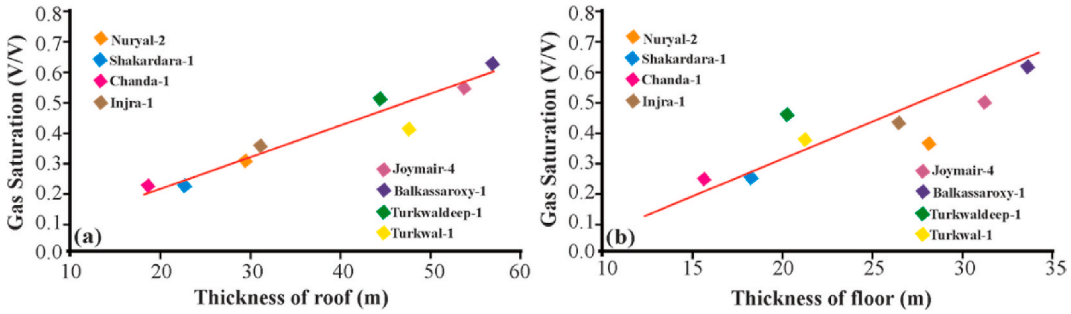


**Fig. 24.** Relationship between the roof and floor thickness variation and gas saturation; (a) gas saturation versus thickness of roof (top) stratum, (b) gas saturation versus thickness of floor (bottom) stratum.

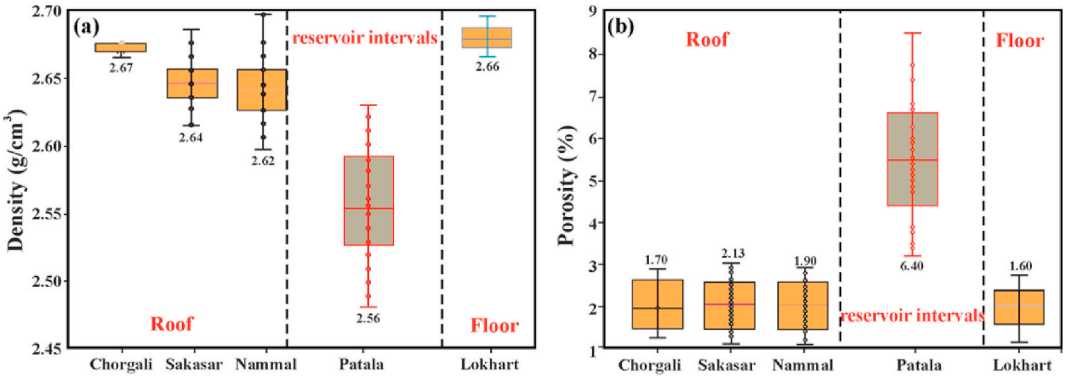


**Fig. 25.** Variation of density and porosity in the roof (Nammal, Sakassar and Chorgali Formations) and floor (Lokhart Formation) in the Turkwal-1 and Joyamair-4 well (Appendix A), (a) density-box-plots; (b) porosity-box-plots.

the majority of the examples given in the literature show that tight limestone are the best for sealing the shale gas reservoir due to their very low porosity and permeability, high density, and high water saturation (Liang et al., 2011; Zagorski et al., 2012; Guo, 2013; Guo and Zeng, 2015; Tang et al., 2020).

In the following paragraphs, we discuss the sealing effectiveness of roof and floor for Patala shale in complex structural areas from five different perspectives: lithology, thickness, density, porosity, and permeability.

**Lithology:** The sealing model of the roof and floor for shale gas preservation and enrichment in Patala Formation is developed and presented in Fig. 23. The underlying stratum of the Patala shale is the Lockhart Formation which is composed of tight and compacted limestone. This underlying stratum is acting as a floor. The overlying stratum is also composed of tight and compacted limestone from Nammal, Sakassar and Chorgali Formation, acting as a roof. Previous studies have proved that lithology play an important role on the sealing capacity of the roof and floor (Downey, 1984; Ingram and Urai, 1999; Dawson and Almon, 2002;. Lash, 2006). The tight carbonate beds of the Triassic in the Sichuan Basin are likewise acting as the regional caprocks for the WF-LM shale gas (Guo and Zeng, 2015; Tang et al., 2020).

**Thickness:** Previous studies show that the thickness of the underlying and overlying stratum of shale gas reservoir can maintain a good sealing capacity to accumulate abundance of natural gas (Guo and Ping, 2015). The studies also prove that tight and stable distribution of floor and the thick roof provide strong sealing for shale gas retention and accumulation (Guo, 2013; Tang et al., 2020). In Fig. 23, the thickness of the Patala Formation is 20–40 m while the thickness of Lockhart Formation (floor) is 20–30 m. The Nammal, Sakassar and Chorgali Formation (roof) reach a maximum thickness of 40–60 m, which is much thicker than Patala Formation and form multi-layers sealing beds. The relationship between the roof and floor thickness variations and gas saturation in the all eight wells show positive correlation, i.e., the gas saturation increases as the thickness of the roof and floor (Fig. 24). Guo and Ping (2015) reported the adverse impact of roof stratum thicknesses below 40–50 m and floor stratum thickness less or equal to 20 m on shale gas retention and accumulation.

**Porosity:** The sealing ability of an effective roof and floor is also closely associated with porosity, permeability, density, water saturation, and micropore structure (Fig. 25a and b) (Guo and Ping, 2015). The average porosity of Patala shale in the Turkwal-1 and Joyamair-4 wells is high (4.4% and 6.4%, respectively) as shown in Fig. 25b, while the porosities of the floor (Lokhart Formation) and the roof (set of Nammal, Sakassar and Chorgali Formation) are low (average of 1.60%; 1.9%, 2.1%, and 1.7%, respectively; Appendix A, Table 1).

The porosity variation produces capillary pressure along the boundaries between the organic-rich shale intervals and the roof/floor, preventing gas from naturally migrating upward and build strong physical sealing (Andrews et al., 2009).

Permeability: The average permeability of roof reduces to 0.109 mD and 0.014 mD in Turkwal-1 and Joyamair-4 wells which is also lower than the permeability of Patala shale (Appendix A, Table 1). Likewise, the difference in permeability will create a zone of overpressure just below the impermeable layer. This zone generates an impenetrable hydraulic barrier to all underlying fluids; and inhibits shale gas seepage.

**Density:** The differences in density of rock also have great impact on sealing capacity of the roof and floor, as shown in Fig. 25a. The density of Patala Formation is low (averages of 2.56 g/cm$^3$), with some samples having a density as low as 2.48 g/cm$^3$ (Appendix A, Table 1). However, the compacted limestone in the Lokhart Formation has an average density of approximately 2.65 g/cm$^3$ and act as a floor. On the other hand, the compacted limestone of Nammal, Sakassar and Chorgali Formation, which acting as a roof, are also much tighter than shale of Patala Formation with higher density (Fig. 12).

From the above discussion, we summarize that the lithology, thickness, porosity, permeability, and density of both roof and floor can

**Table 2**
Comparison of key parameters between Patala Formation in Kohat-Potwar plateau and WF-LM Formation in various shale gas fields of China (Guo and Zeng, 2015).

| Region/ Shale Gas Field | Burial Depth (m) | Thickness (m) | TOC (%) | Brittle Minerals (%) | Porosity (%) | Structural Type |
|---|---|---|---|---|---|---|
| Kohat-Potwar | 2200–4500 | 25–145 | 0.6–9.8 | 55 | 2.5–8.5 | Anticline |
| Fuling | 2250–3550 | 38–45 | 2.0–3.9 | 57 | 2.0–4.6 | Anticline |
| Pengshui | 2100–3500 | 24–32 | 2.1–3.3 | 59 | 2.0–5.2 | Syncline |
| Dingshan | 2030–4360 | 26–36 | 3.1–3.8 | 50 | 2.8–5.8 | Anticline |
| Changning | 1500–3500 | 30–32 | 2.0–7.2 | 55 | 4.0–5.0 | Anticlinorium |

provide strong sealing for organic-rich Patala Formation. The sandwiched Patala shale with porosity >6%, TOC >2 (wt. %), burial depth <2500 m, and formation thickness >30 m in the Turkwal-1, Joyamair-4 and Bulkassaroxy-1 wells, laid all the fundamentals for shale gas enrichment in Potwar Plateau (Fig. 23).

Table 2 compares key parameters between the Patala Formation (Pakistan) and WF-LM Formation (China), in different regions. We observe that the assessed parameters in Patala Formation are consistent with those of WF-LM in various shale gas fields of China. Note that structural types and regional tectonic framework are the key factors for shale gas preservation and enrichment in shale gas fields of China. Literature review on Marcellus, Haynesville, and Barnett gas fields indicate that the gas pools contributed significantly to free gas, up to 70–80%. Also, the free gas content in the Fuling shale gas field was 55–65% (Liang et al., 2011; Zagorski et al., 2012; Guo, 2013; Guo and Zeng, 2015; Tang et al., 2020). Thus, the shale gas is predominantly free gas and there is no faults or unconformities inside the shale gas zone to provide migration channels. Nevertheless, Guo and Zeng (2015) reported that short-distance migration is still possible due to inter-well interference during fracturing in the Jiaoshiba shale gas field.

## 5. Conclusion

The evaluation of shale gas reservoirs in complex structural enclosures using well logs and seismic survey provided a detailed understanding of fundamental elastic and petrophysical properties, Rock-Eval pyrolysis, and sealing mechanism of shale in the Kohat-Potwar Plateau, Pakistan. The following conclusions can be drawn from this study:

1. In addition to reservoir properties of Patala Formation, the structural style and favorable preservation conditions are the main factors controlling shale gas accumulation. The underlying and overlying stratum of Patala Formation, consisting of compacted limestone with low porosity (typically less than 3%) and ultra-low permeability, high density, and large thicknesses provide high-efficient sealing that ensure favorable preservation conditions of shale gas.
2. The sandwiched Patala shale has relatively high organic matter content and stable thermal maturation stage (TOC > 2%, $T_{max}$ about 416–445 °C, kerogen type-II and III), high weight percentage of calcite and dolomite contents (with the majority of data points falling in the brittle region), porosity > 6%, burial depth < 2500 m, and formation thickness > 30 m. However, the geochemical evaluation revealed that the maturity of Patala Formation is in immature to early maturate stage.
3. The petrophysical characteristics of the Patala Formation are remarkably similar to the reservoir properties of WF-LM Formation in various shale gas fields of China. These characteristics laid the fundamental basis for large-scale shale resource exploration in the Kohat-Potwar Plateau.
4. Furthermore, the multiphase tectonic evolution in the Kohat-Potwar Plateau provides various disruptions from Eocene-to-Cambrian to develop fractures and ultimately enhance the porosity and permeability.
5. Although good generative potential, i.e., TOC content, thickness, and brittle mineral content are favorable for shale gas play, complex tectonic evolution in Kohat-Potwar Plateau and insufficient maturity constrain the Palata Formation to generate sufficient amount of gas, and hence exploitation from this reservoir could not be economical. However, the whole study can provide a good basis for identifying the sweet spots and preservation condition of shale gas in complex structural enclosures.

## Credit author statement

**Qamar Yasin**: Conceptualization, Methodology, Original Draft Preparation. **Perveiz Khalid**: Geophysical Data Interpretation. **Syrine B.**: Visualization, Investigation of Rock-Eval pyrolysis. **Qizhen Du**: Supervision. **Haroon Ali**: Investigation of petrophysical evaluation. **Cyril Boateng**: Reviewing and Editing the Original Draft.

## Declaration of competing interest

The authors declare that they have no known competing financial interests or personal relationships that could have appeared to influence the work reported in this paper. No competing financial interests

## Acknowledgments

This research is supported by the National Science Foundation of China (41930429, 41574125, and 41774139), the research project of the China National Petroleum Corporation (2019A-33), the China National '111' Foreign Experts Introduction Plan for Tight Oil & Gas Geology and Exploration, and the Deep-Ultradeep Oil & Gas Geophysical Exploration.

## Abbreviations

| | |
|---|---|
| $S_1$ | Free hydrocarbons yield at low temperature, mg HC/g rock (it represents the bitumen in the rock or the fraction of the initial petroleum potential) |
| $S_2$ | Hydrocarbons yield from cracking of kerogen, mg HC/g rock (it represents the kerogen or the residual petroleum potential) |
| $S_3$ | $CO_2$ yield, mg $CO_2$/g rock |
| $T_{max}$ | Temperature at which maximum hydrocarbons yield, deg C |
| HI | Hydrogen index = $S_2 \times 100$/TOC, mg HC/gm TOC |
| OI | Oxygen index = $S_3 \times 100$/TOC, mg $CO_2$/gm TOC |
| PI | Production index = $S_1/S_1+S_2$ (it represents the quantity of bitumen produced by the maturation of the kerogen) |
| BI | Brittleness index |

## Appendix A

**Table 1**
Laboratory-measured petrophysical properties of Nammal, Sakassar, Chorgali, and Lokhart Formation in the Kohat-Potwar Plateau.

| No | Well | Porosity | Permeability | | Density | | Saturation | | Carbonate Content | |
|---|---|---|---|---|---|---|---|---|---|---|
| | | | Horizontal | Vertical | Bulk | Grain | (%) | | (%) | |
| | | (%) | (mD) | (mD) | gm/cc | gm/cc | Oil | Water | Calcite | Dolomite |
| 1 | Tukwal-1 | 1.8 | 0.005 | 0.004 | 2.62 | 2.68 | 71.00 | 0.10 | 72 | 3 |
| 2 | Tukwal-1 | 2.1 | 0.005 | 0.003 | 2.63 | 2.69 | 62.00 | 0.97 | 70 | 3.5 |
| 3 | Tukwal-1 | 1.8 | 0.100 | 0.006 | 2.66 | 2.70 | 34.00 | 0.15 | 90 | 6 |
| 4 | Tukwal-1 | 1.2 | 0.005 | 0.004 | 2.66 | 2.69 | 85.00 | 0.06 | 85 | 5 |
| 5 | Tukwal-1 | 2.1 | 0.005 | 0.004 | 2.63 | 2.69 | 31.00 | 0.72 | 89 | 5 |
| 6 | Tukwal-1 | 1.3 | 0.005 | 0.004 | 2.68 | 2.71 | 11.00 | 0.67 | 94 | 4 |
| 7 | Tukwal-1 | 1.6 | 0.005 | 0.004 | 2.68 | 2.72 | 26.00 | 0.12 | 90 | 8 |
| 8 | Tukwal-1 | 2.2 | 0.005 | 0.004 | 2.67 | 2.73 | 13.00 | 0.61 | 96 | 1.5 |
| 9 | Tukwal-1 | 1.3 | 0.005 | 0.004 | 2.68 | 2.71 | 18.00 | 0.01 | 97 | 2.5 |
| 10 | Tukwal-1 | 1.7 | 0.005 | 0.004 | 2.67 | 2.72 | 31.00 | 0.80 | 82 | 10 |
| 11 | Tukwal-1 | 1.1 | 0.005 | 0.004 | 2.68 | 2.71 | 25.00 | 0.76 | 87 | 10 |
| 12 | Tukwal-1 | 1.2 | 0.050 | 0.010 | 2.68 | 2.71 | 22.00 | 0.53 | 94 | 3.5 |
| 13 | Tukwal-1 | 1.6 | 0.050 | 0.020 | 2.66 | 2.70 | 35.00 | 0.63 | 92 | 6 |
| 14 | Tukwal-1 | 1.8 | 0.050 | 0.020 | 2.66 | 2.71 | 26.00 | 0.23 | 96 | 0 |
| 15 | Tukwal-1 | 1.5 | 0.005 | 0.003 | 2.66 | 2.70 | 19.00 | 0.10 | 78 | 0 |
| 16 | Tukwal-1 | 1.7 | 0.100 | 0.005 | 2.65 | 2.69 | 40.00 | 0.93 | 88 | 2 |
| 17 | Tukwal-1 | 1.9 | 0.005 | 0.003 | 2.62 | 2.68 | 37.00 | 0.70 | 82 | 2 |
| 18 | Tukwal-1 | 2.6 | 0.005 | 0.003 | 3.18 | 3.26 | 23.00 | 0.92 | 84 | 2 |
| 19 | Tukwal-1 | 1.7 | 0.100 | 0.005 | 2.64 | 2.69 | 55.00 | 0.27 | 82 | 2 |
| 20 | Tukwal-1 | 1.4 | 0.005 | 0.003 | 2.68 | 2.72 | 36.00 | 0.87 | 90 | 0 |
| 21 | Tukwal-1 | 2.1 | 2.300 | 0.010 | 2.66 | 2.72 | 8.00 | 0.90 | 96 | 0 |
| 22 | Tukwal-1 | 1.4 | 0.100 | 0.005 | 2.69 | 2.72 | 31.00 | 0.90 | 82 | 0 |
| 23 | Tukwal-1 | 1.5 | 0.100 | 0.200 | 2.67 | 2.71 | 26.00 | 0.03 | 86 | 2 |
| 24 | Tukwal-1 | 1.6 | 0.005 | 0.003 | 2.68 | 2.72 | 19.00 | 0.04 | 80 | 2 |
| 25 | Tukwal-1 | 1.3 | 0.005 | 0.003 | 2.67 | 2.70 | 38.00 | 0.57 | 78 | 0 |
| 26 | Tukwal-1 | 1.6 | 0.005 | 0.003 | 2.68 | 2.72 | 19.00 | 0.04 | 72 | 8 |
| 27 | Tukwal-1 | 1.5 | 0.005 | 0.004 | 2.67 | 2.71 | 18.00 | 0.81 | 82 | 0 |
| 28 | Tukwal-1 | 1.4 | 0.005 | 0.004 | 2.65 | 2.69 | 30.00 | 0.44 | 80 | 0 |
| 1 | Joyamair-4 | 0.8 | 0.01 | 0 | 2.68 | 2.7 | 42.0 | 6.2 | 88 | 6 |
| 2 | Joyamair-4 | 1.2 | 0.01 | 0 | 2.66 | 2.69 | 4.4 | 15.5 | 94 | 2 |
| 3 | Joyamair-4 | 0.8 | 0.01 | 0 | 2.66 | 2.68 | 19.0 | 0.6 | 81 | 10 |
| 4 | Joyamair-4 | 1.1 | 0.01 | 0 | 2.63 | 2.68 | 28.0 | 1.0 | 94 | 2 |
| 6 | Joyamair-4 | 1.0 | 0.01 | 0 | 2.67 | 2.7 | 0.5 | 0.1 | 92 | 5 |
| 7 | Joyamair-4 | 1.2 | 0.01 | 0 | 2.66 | 2.69 | 7.2 | 13.0 | 88 | 6 |
| 8 | Joyamair-4 | 0.7 | 0.10 | 0 | 2.69 | 2.71 | 20.0 | 1.0 | 84 | 7 |
| 9 | Joyamair-4 | 1.6 | 0.01 | 0 | 2.66 | 2.71 | 25.0 | 0.2 | 86 | 9 |
| 10 | Joyamair-4 | 1.3 | 0.01 | 0 | 2.66 | 2.7 | 18.0 | 0.6 | 90 | 7 |
| 11 | Joyamair-4 | 2.1 | 0.01 | 0 | 2.66 | 2.73 | 5.0 | 0.1 | 94 | 3 |
| 12 | Joyamair-4 | 1.0 | 0.01 | 0 | 2.67 | 2.69 | 22.0 | 1.0 | 95 | 3 |
| 13 | Joyamair-4 | 1.7 | 0.01 | 0 | 2.65 | 2.70 | 4.7 | 42.0 | 84 | 12 |
| 14 | Joyamair-4 | 0.9 | 0.01 | 0 | 2.65 | 2.68 | 2.0 | 54.0 | 74 | 15 |
| 15 | Joyamair-4 | 1.4 | 0.01 | 0 | 2.66 | 2.69 | 0.8 | 23.0 | 84 | 8 |
| 17 | Joyamair-4 | 2.1 | 0.01 | 0 | 2.67 | 2.73 | 7.2 | 9.6 | 90 | 7 |
| 18 | Joyamair-4 | 1.3 | 0.01 | 0 | 2.67 | 2.7 | 23.0 | 0.1 | 86 | 12 |
| 19 | Joyamair-4 | 1.1 | 0.02 | 0 | 2.66 | 2.69 | 6.0 | 1.0 | 68 | 17 |
| 20 | Joyamair-4 | 0.5 | 0.01 | 0 | 2.72 | 2.73 | 4.2 | 29.2 | 78 | 15 |
| 21 | Joyamair-4 | 1.6 | 0.01 | 0 | 2.65 | 2.7 | 16.0 | 0.3 | 92 | 5 |
| 22 | Joyamair-4 | 1.4 | 0.01 | 0 | 2.65 | 2.69 | 28.0 | 0.8 | 90 | 6 |
| 23 | Joyamair-4 | 1.9 | 0.02 | 0 | 2.64 | 2.69 | 32.0 | 1.0 | 82 | 14 |
| 24 | Joyamair-4 | 2.8 | 0.01 | 0 | 2.6 | 2.7 | 4.3 | 3.8 | 95 | 3 |
| 25 | Joyamair-4 | 1.6 | 0.01 | 0 | 2.67 | 2.71 | 18.8 | 4.2 | 82 | 14 |
| 26 | Joyamair-4 | 1.5 | 0.01 | 0 | 2.65 | 2.69 | 35.3 | 4.5 | 72 | 19 |
| 28 | Joyamair-4 | 1.3 | 0.01 | 0 | 2.67 | 2.71 | 25.0 | 4.6 | 90 | 6 |
| 29 | Joyamair-4 | 1.3 | 0.01 | 0 | 2.70 | 2.73 | 52.0 | 10.4 | 60 | 36 |

## References


Ayaz, A.S., Haider, B.A., Ismail, K., Smith, P.M., 2012. Unconventional Hydrocarbon Resource Plays in Pakistan: an Overview Awakening a South East Asian Sleeping Giant-Technological Solutions to Unlock the Vast Unconventional Reserves of Pakistan. Search and Discovery Article #80216.

Ali, A., Ullah, M., Hussain, M., Asher, S., 2017. Estimation of the shale oil/gas potential of a paleocene–eocene succession: a case study from the meyal area, potwar basin, Pakistan. Acta Geol. Sin. 91 (6), 2180–2199.

Almon, W.R., Dawson, W.C., Sutton, S.J., Ethridge, F.G., Castelblanco, B., 2002. Sequence Stratigraphy, Facies Variation and Petrophysical Properties in Deepwater Shales, Upper Cretaceous Lewis Shale, South-Central Wyoming.

Ahmed, S.A., 2003. Comparative study of structural styles in Kohat Plateau, NW himalayans, NWFP, Pakistan. Ph.D. Thesis. National Center of Excellence in Geology (NCEG), University of Peshawar, Peshawar, Pakistan.

Aamir, M., Siddiqui, M.M., 2006. Interpretation and visualization of thrust sheets in a triangle zone in eastern Potwar, Pakistan. Lead. Edge 25 (1), 24–37.

Abd-Allah, Z.M., Wan Hasiah, Abdullah, Abdel-Fattah, M.I., 2019. Assessment of Eocene, Paleocene and cretaceous source rocks in the west feiran area, offshore gulf of suez, Egypt. J. Petrol. Sci. Eng. 180, 756–772.

Abdel-Fattah, M., Pigott, J., Abd-Allah, Z.M., 2017. Integrative 1D-2d basin modeling of the cretaceous beni suef basin, western desert, Egypt. J. Petrol. Sci. Eng. 153, 297–313.

Abd-Allah, Z.M., Abubakr, F., Maky, Ramadan, M.A.M., 2018. Organic source of crude oils and 1d basin modeling of upper cretaceous rocks, badr concession, abu gharadig basin, western desert, Egypt. Arabian J. Geosci. 11, 13P.

Ahmed, et al., 2019. Precise seismic substructural model of the Eocene Chorgali limestone in the turkwal oil field, central potwar, Pakistan. Acta Geol. Sin. 93 (6), 1711–1720. https://doi.org/10.1111/1755-6724.13813.
Alexeyev, A., Ostadhassan, M., Mohammed, R.A., et al., 2017. Well log based geomechanical and petrophysical analysis of the bakken formation. 51st US Rock Mechanics/Geomechanics Symposium. American Rock Mechanics Association.
Ali, S.H., 2009a. Lithostructural Mapping of Ara-Basharat Area Eastern Salt Range with Special Emphasize on Bioturbations of the Kussak Formation and Reservoir Characteristics of the Baghanwala Formation, Eastern Salt Range, Pakistan. M.Sc. Thesis, University of the Punjab, Lahore.
Ali, S.H., 2009b. Reservoir characteristics of early-middle cambrian baghanwala formation eastern salt range Pakistan. In: SPE and PAPG Annual Technical Conference, Maximize Reserves – Optimize Exploitation, November 17-18, Islamabad.
Andrews, A., Folger, P., Humphries, M., et al., 2009. Unconventional gas shales: development, technology, and policy issues. Congr. Res. Serv. 7, R40894. www.crs.gov.
Crain, R.E., Holgate, D., 2014. A 12-step Program to Reduce Uncertainty in Kerogen-Rich Reservoirs: FOCUS, GeoConvention, pp. 1–11.
Dai, J., Zou, C., Liao, S., et al., 2014. Geochemistry of the extremely high thermal maturity Longmaxi shale gas, southern Sichuan basin. Org. Geochem. 74, 3–12.
Downey, M.W., 1984. Evaluating seals for hydrocarbon accumulations. AAPG Bull. 68 (11), 1752–1763.
Dawson, W.C., Almon, W.R., 2002. Top Seal Potential of Tertiary Deep-Water Gulf of Mexico Shales.
Espitalié, J., Deroo, G., Marquis, F., 1985. La pyrolyse Rock-Eval et ses applications. Deuxième partie. Rev. Inst. Fr. Petrol 40 (6), 755–784.
Fazeelat, T., Jalees, M.I., Bianchi, T.S., 2010. Source rock potential of Eocene, Paleocene and Jurassic deposits in the subsurface of the Potwar basin, northern Pakistan. J. Petrol. Geol. 33 (1), 87–96.
Fatmi, A.N., 1973. Lithostratigraphic units of the kohat-potwar province Indus Basin, Pakistan. Mem. Geol. Surv. Pak. 10, 1–180.
Fakhri, M., Tabatabaei, H., Amiri, A., 2013. Comparing the potential of hydrocarbon generation of kazhdomi and pabdeh formations in bangestan anticline (zagros basin) according to rock-eval pyrolysis data. J. Earth Sci. Climatic Change 4, 7P.
Fu, X., Wu, T., Lyu, Y., Liu, S., Tian, H., Lu, M., 2018. Research status and development trend of the reservoir caprock sealing properties. Oil Gas Geol. 39 (3), 454–471.
Guo, T., 2013. Evaluation of highly thermally mature shale-gas reservoirs in complex structural parts of the Sichuan Basin. J. Earth Sci. 24, 863–873. https://doi.org/10.1007/s12583-013-0384-4.
Guo, T., Zeng, P., 2015. The structural and preservation conditions for shale gas enrichment and high productivity in the Wufeng–Longmaxi Formation, Southeastern Sichuan Basin. Energy Explor. Exploit. 33 (3), 259–276.
Guo, X., Hu, D., Li, Y., Wei, Z., Wei, X., Liu, Z., 2017. Geological factors controlling shale gas enrichment and high production in Fuling shale gas field. Petrol. Explor. Dev. 44 (4), 513–523.
Ghazi, S., Ali, S.H., Sahraeyan, M., Hanif, T., 2015. An overview of tectonosedimentary framework of the Salt Range, northwestern Himalayan fold and thrust belt, Pakistan. Arabian J. Geosci. 8 (3), 1635–1651.
Ghazi, S., Ali, S.H., Shahzad, T., Ahmed, N., Perveiz, K., Akram, S., Ali, S., Sami, J., 2020. Sedimentary, structural and salt tectonic evolution of karoli-nilawahan area, central salt range and its impact for the potwar province. Himal. Geol. 41 (2), 145–156.
Ghori, K.A., Haines, P.W., 2007. Paleozoic Petroleum Systems of the Canning Basin, Western Australia (Abs): a Review. AAPG International Conference and Exhibition, Perth, Western Australia.
Hunt, J.M., 1996. Petroleum Geochemistry and Geology, second ed. Freeman and Company, New York, p. 743P.
Huang, J.L., Zou, C.N., Li, J.Z., 2012. Shale gas generation and potential of the lower cambrian qiongzhusi formation in the southern Sichuan basin, China. Petrol. Explor. Dev. 39 (1), 75–81.
Huang, Z., Hao, S., 1996. Study on sealing of gas concentration and difussion in overlying gas reservoirs. Acta Pet. Sin. 847, 4.
Ingram, G.M., Urai, J.L., 1999. Top-seal leakage through faults and fractures: the role of mudrock properties. Geological Society, London, Special Publications 158 (1), 125–135.
Iqbal, O., Ahmad, M., Abd Kadir, A., 2018. Effective evaluation of shale gas reservoirs by means of an integrated approach to petrophysics and geomechanics for the optimization of hydraulic fracturing: a case study of the Permian Roseneath and Murteree Shale Gas reservoirs, Cooper Basin, Australia. J. Nat. Gas Sci. Eng. 58, 34–58.
Jin, Z., Nie, H., Liu, Q., Zhao, J., Jiang, T., 2018. Source and seal coupling mechanism for shale gas enrichment in upper ordovician Wufeng Formation-lower silurian Longmaxi formation in Sichuan basin and its periphery. Mar. Petrol. Geol. 97, 78–93.
Jiang, S., Mokhtari, M., Borrok, D., Lee, J., 2018. Improving the total organic carbon estimation of the eagle ford shale with density logs by considering the effect of pyrite. Minerals 8 (4), 154. http://doi:10.3390/min8040154.
Jalees, I.M., Tahira, F., 2020. Geochemical segregation of early Permian, Paleocene and Eocene sediments of Potwar Basin, Pakistan: I Geophysical and isotopic analysis for source and depositional environment. Carbonates Evaporites 35 (63). https://doi.org/10.1007/s13146-020-00597-2.
Khan, N., Anjum, N., Ahmad, M., Awais, M., 2018. Hydrocarbon source rock potential evaluation of the late Paleocene Patala formation, salt range, Pakistan: organic geochemical and palynofacies approach. J. Earth Syst. Sci. 127 https://doi.org/10.1007/s12040-018-0998-0.
Khan, S.D., Cen, L., Ahmad, S., Ahmad, I., Ali, F., 2012. Lateral structural variation along the Kalabagh fault zone, NW Himalayan foreland fold-and-thrust belt, Pakistan. J. Asian Earth Sci. 50, 79–87.
Khalid, P., Qayyum, F., Yasin, Q., 2014. Data-driven sequence stratigraphy of the cretaceous depositional system, Punjab platform, Pakistan. Surv. Geophys. 35, 1065–1088. https://doi.org/10.1007/s10712-014-9289-8.
Kim, T., Seho, H., Jang, S., 2017. Petrophysical approach for S-wave velocity prediction based on brittleness index and total organic carbon of shale gas reservoir: a case study from Horn River Basin, Canada. J. Appl. Geophys. 136, 513–520.
Katz, S.A., Chilingarian, G.V., Islam, M.R., 1995. Estimation of reservoir porosity and saturations using multiple sources of geophysical data. J. Petrol. Sci. Eng. 13, 103–111. https://doi.org/10.1016/0920-4105(95)00004-2.
Law, B.E., Shah, S.H.A., Malik, M.A., 1998. Abnormally high formation pressures, Potwar Plateau, Pakistan. In: Law, B.E., Ulmishek, G.F., Slavin, V.I. (Eds.), Abnormal Pressures in Hydrocarbon Environments, vol. 70. American Association of Petroleum Geologists Memoir, pp. 247–258.
Li, Z., Li, L., Li, M., Zhang, L., Zhang, Z., Huang, B., Tang, C., 2018. A numerical investigation on the effects of rock brittleness on the hydraulic fractures in the shale reservoir. J. Nat. Gas Sci. Eng. 50, 22–32.
Liang, X., Ye, X., Zhang, J.H., Shu, H.L., Lou, J.S., Yao, Q.C., Wang, G.C., 2011. Reservoir forming conditions and favorable exploration zones of shale gas in the Weixin Sag, Dianqianbei Depression. Petrol. Explor. Dev. 38 (6), 693–699.
Li, Y., Wang, X., Wu, B., Li, G., Wang, D., 2016. Sedimentary facies of marine shale gas formations in southern China: the lower silurian Longmaxi formation in the southern Sichuan basin. J. Earth Sci. 27 (5), 807–822.
Liang, C., Jiang, Z.X., Yang, Y.T., Wei, X.J., 2012. Shale lithofacies and reservoir space of the Wufeng Longmaxi formation, Sichuan basin, China. Petrol. Explor. Dev. 39 (6), 736–743.
Liang, C., Jiang, Z.X., Yang, Y.T., Zhang, C., 2016. Deep-water depositional mechanisms and significance for unconventional hydrocarbon exploration: a case study from the lower Silurian Longmaxi shale in the southeastern Sichuan Basin. AAPG (Am. Assoc. Pet. Geol.) Bull. 100 (5), 773–794.
Lash, G.G., 2006. Top seal development in the shale-dominated upper devonian catskill delta complex, western New York state. Mar. Petrol. Geol. 23 (3), 317–335.
Makky, A.F., Mohamed, I., El Sayed, Ahmed, S., Abu, El-Ata, Ibrahim, M., Abd El-Gaied, Mohamed, I., Abdel-Fattah, Zakaria, M., Abd-Allah, 2014. Source rock evaluation of some upper and lower cretaceous sequences, west beni suef concession, western desert, Egypt. Egypt. J. Pet. 23, 139–145.
Mashhadi, Z.S., Rabbani, A.R., Kamali, M.R., Mirshahani, M., Khajehzadeh, A., 2015. Burial and thermal maturity modeling of the Middle Cretaceous–Early Miocene petroleum system, Iranian sector of the Persian Gulf. Petrol. Sci. 12 (3), 367–390.
Mavko, G., Mukerji, T., Dvorkin, J., 2009. The Rock Physics Handbook: Tools for Seismic Analysis of Porous Media. Cambridge university press.
Meissner, C.R., Master, J.M., Rashid, M.A., Hussain, M., 1974. Stratigraphy of Kohat Quadrangle, Pakistan. United States Geological Survey Reston, VA, USA. Professional Paper, 716–D.
Nazir, A., Iqbal, M., Siddique, A., Ahmed, W., 2020. Evaluation of source, depositional environment, thermal maturity and biodegradation of organic matter from Kohat-Potwar Basin, Pakistan. Petrol. Sci. Technol. 38 (2), 106–115.
Paracha, W., 2004. Kohat plateau with reference to Himalayan tectonic general study. CSEG recorder.
Peters, K.E., Cassa, M.R., 1994. Applied source rock geochemistry. In: Magoon, L.B., Dow, W.G. (Eds.), The Petroleum System—From Source to Trap. American Association of Petroleum Geologists Memoir, pp. 93–120.
Peters, K.E., Magoon, L.B., Bird, K.J., Valin, Z.C., Keller, M.A., 2006. North Slope, Alaska: source rock distribution, richness, thermal maturity, and petroleum charge. AAPG (Am. Assoc. Pet. Geol.) Bull. 90, 261–292.
Peters, K.E., 1986. Guidelines for evaluating petroleum source using programmed pyrolysis. AAPG (Am. Assoc. Pet. Geol.) Bull. 70, 318–329.
Passey, Q., Creaney, S., Kulla, J., et al., 1990. A practical model for organic richness from porosity and resistivity logs. AAPG (Am. Assoc. Pet. Geol.) Bull. 74 (12), 1777–1794.
Pivnik, D.A., Wells, N.A., 1996. The translation from tethys to the himalaya as recorded in northwest Pakistan. Geol. Soc. Am. Bull. 108, 1295–1311.
Pogue, K.R., Hylland, M.D., Yeats, R.S., Khattak, W.U., Hussain, A., 1999. Stratigraphic and Structural Framework of Himalayan Foothills, Northern Pakistan. Special Papers-Geological Society of America, pp. 257–274.
Soua, M., 2014. Paleozoic oil/gas shale reservoirs in southern Tunisia: an overview. J. Afr. Earth Sci. 100, 450–492.
Schmoker, J.W., Hester, T.C., 1983. Organic carbon in bakken formation, United States portion of williston basin. AAPG (Am. Assoc. Pet. Geol.) Bull. 67 (12), 2165–2174.
Sohail, G.M., Hawkes, C.D., 2020. An evaluation of empirical and rock physics models to estimate shear wave velocity in a potential shale gas reservoir using wireline logs. J. Petrol. Sci. Eng. 185 (106666) https://doi.org/10.1016/j.petrol.2020.108225.
Sohail, G.M., Hawkes, C.D., Yasin, Q., 2020. An integrated petrophysical and geomechanical characterization of Sembar Shale in the Lower Indus Basin, Pakistan, using well logs and seismic data. J. Nat. Gas Sci. Eng. 78 https://doi.org/10.1016/j.jngse.2020.103327.
Shah, S.M.I., 2009. Stratigraphy of Pakistan; govt. Pak. Ministry of petrol. Nat. Resour. Geol. Surv. Pak. 22 (1–5), 243–244.
Shah, S.M.I., Ahmed, R., Cheema, M.R., Fatmi, A.N., Iqbal, M.W.A., Raza, H.A., Raza, S. M., 1977. Stratigraphy of Pakistan: geological survey of Pakistan. Memoir 12, 137p.
Shazly, T., Ramadan, M., El-Sawy, M., 2013. Application of well logs analysis to identify the source rock capabilities of rudeis and kareem formations in rudeis field, gulf of suez, Egypt. J. Appl. Sci. Res. 9.

Shalaby, M.R., Hakimi, M.H., Abdullah, W.H., 2012. Modeling of gas generation from the alam el-bueib formation in the shoushan basin, northern western desert of Egypt. Int. J. Earth Sci. 102, 319–332.

Shia, X., Liu, G., Cheng, Y., Yang, L., Jiang, H., Chen, L., Jiang, S., Wang, J., 2016. Brittleness index prediction in shale gas reservoirs based on efficient network models. J. Nat. Gas Sci. Eng. 35, 673–685.

Sharma, V., Sircar, A., 2018. Integrated petrophysical and geomechanical characterization of cambay shale, cambay basin, India. In: Research and Development Petroleum Conference and Exhibition, vol. 2018. European Association of Geoscientists & Engineers, pp. 107–109.

Song, Y., Li, Z., Jiang, Z., Luo, Q., Liu, D., Gao, Z., 2017. Progress and development trend of unconventional oil and gas geological research. Petrol. Explor. Dev. 44 (4), 675–685.

Tissot, B.P., Welte, D.H., 1984. Petroleum Formation and Occurrence, second ed. Springer, New York, p. 699.

Tang, L., Song, Y., Jiang, S., et al., 2020. Sealing mechanism of the roof and floor for the Wufeng-Longmaxi shale gas in the southern Sichuan Basin. Energy Fuels. https://doi.org/10.1021/acs.energyfuels.0c00983.

Tang, X., Jiang, Z., Jiang, S., et al., 2019. Characteristics, capability, and origin of shale gas desorption of the Longmaxi Formation in the southeastern Sichuan Basin, China. Sci. Rep. 9, 1035. https://doi.org/10.1038/s41598-018-37782-2.

Vernik, L., Liu, X., 1997. Velocity anisotropy in shales: a petrophysical study. Geophysics 62, 521–532.

Waples, D.W., 1985. Geochemistry in Petroleum Exploration. Inter. Human Resources and Develop. Co., Boston, p. 232.

Watts, N., 1987. Theoretical aspects of cap-rock and fault seals for single-and two-phase hydrocarbon columns. Mar. Petrol. Geol. 4 (4), 274–307.

Wandrey, C.J., Law, B.E., Shah, H.A., 2004. Patala-Nammal composite total petroleum system, Kohat-Potwar geologic province, Pakistan, United States Department of the Interior. US Geol. Surv. Bull. 2208 (C), 2–10.

Warwick, P.D., Shakoor, T., 1993. Lithofacies and Depositional Environments of the Coal-Bearing Paleocene Patala Formation, Salt Range Coal FIeld, Northern Pakistan, vol. 5. Geological Survey of Pakistan, Project Report (IR) PK-109, p. 52.

Wei, X., Li, Y., Wei, Z., Liu, R., Yu, G., Wang, Q., 2017. Effects of preservation conditions on enrichment and high yield of shale gas in Sichuan Basin and its periphery. Pet. Geol. Exp. 39 (2), 147–153.

Wu, Y., Li, X., He, J., Zheng, B., 2016. Mechanical properties of Longmaxi black organic-rich shale samples from south China under uniaxial and triaxial compression states. Energies 9, 1088.

Yasin, Q., Sohail, G.M., Du, Q., 2020a. Application of machine learning tool to predict the porosity of clastic depositional system, Indus Basin, Pakistan. J. Petrol. Sci. Eng. 107975. https://doi.org/10.1016/j.petrol.2020.107975.

Yasin, Q., Sohail, G.M., Du, Q., 2020b. Estimation of petrophysical parameters from seismic inversion by combining particle swarm optimization and multilayer linear calculator. Nat. Resour. Res. 29, 3291–3317. https://doi.org/10.1007/s11053-020-09641-3.

Yasin, Q., Du, Q., Sohail, G.M., Ismail, A., 2017. Impact of organic contents and brittleness indices to differentiate the brittle-ductile transitional zone in shale gas reservoir. Geosci. J. 21 (5), 779–789.

Yasin, Q., Du, Q., Sohail, G.M., Ismail, A., 2018. Fracturing index-based brittleness prediction from geophysical logging data: application to Longmaxi shale. GeoMech. Geophys. Geo-Energy Geo-Resources 4 (4), 301–325.

Yu, L., Fan, M., Liu, W., Zhang, W., Chen, H., 2011. Seal mechanism of cap rocks. Pet. Geol. Exp. 1.

Zhang, K., Song, Y., Jiang, S., Jiang, Z., Jia, C., Huang, Y., Liu, X., Wen, M., Wang, X., Li, X., 2019a. Shale gas accumulation mechanism in a syncline setting based on multiple geological factors: an example of southern Sichuan and the Xiuwu Basin in the Yangtze Region. Fuel 241, 468–476.

Zhang, K., Song, Y., Jia, C., Jiang, Z., Jiang, S., Huang, Y., Wen, M., Liu, X., Liu, W., Chen, Z., Xie, X., Liu, T., Wang, X., Wang, P., Li, X., Shan, C., 2019b. Vertical sealing mechanism of shale and its roof and floor and effect on shale gas accumulation, a case study of marine shale in Sichuan basin, the Upper Yangtze area. J. Petrol. Sci. Eng. 175, 743–754.

Zhang, C., Dong, D., Wang, Y., Guan, Q., 2017. Brittleness evaluation of the upper ordovician wufeng–lower silurian Longmaxi shale in southern Sichuan basin, China. Energy Explor. Exploit. 35 (4), 430–443.

Zhu, L., Zhang, C., Guo, C., Jiao, Y., Chen, L., Zhou, X., Zhang, C., Zhang, Z., 2018. Calculating the total porosity of shale reservoirs by combining conventional logging and elemental logging to eliminate the effects of gas saturation. Petrophysics 59 (2), 162–184.

Zagorski, W.A., Wrightstone, G.R., Bowman, D.C., 2012. The Appalachian Basin Marcellus gas play: its history of development, geologic controls on production, and future potential as a world-class reservoir. In: Breyer, J.A. (Ed.), Shale Reservoirs-Giant Resources for the 21st Century, vol. 97. AAPG Memoir, pp. 172–200.